Heating Hot Atmospheres with Active Galactic Nuclei

B. R. McNamara
Department of Physics & Astronomy, University of Waterloo, Ontario, Canada, Astrophysical Institute and Department of Physics and Astronomy, Ohio University, Athens, OH 45701, and Harvard-Smithsonian Center for Astrophysics, 60 Garden Street, Cambridge, MA 02138

P. E. J. Nulsen
Harvard-Smithsonian Center for Astrophysics, 60 Garden Street, Cambridge, MA 02138

Key Words active galactic nuclei, cooling flows, galaxy clusters, radio galaxies, X-ray emission

Abstract High resolution X-ray spectroscopy of the hot gas in galaxy clusters has shown that the gas is not cooling to low temperatures at the predicted rates of hundreds to thousands of solar masses per year. X-ray images have revealed giant cavities and shock fronts in the hot gas that provide a direct and relatively reliable means of measuring the energy injected into hot atmospheres by active galactic nuclei (AGN). Average radio jet powers are near those required to offset radiative losses and to suppress cooling in isolated giant elliptical galaxies, and in larger systems up to the richest galaxy clusters. This coincidence suggests that heating and cooling are coupled by feedback, which suppresses star formation and the growth of luminous galaxies. How jet energy is converted to heat and the degree to which other heating mechanisms are contributing, eg. thermal conduction, are not well understood. Outburst energies require substantial late growth of supermassive black holes. Unless all of the $\sim 10^{62}$ erg required to suppress star formation is deposited in the cooling regions of clusters, AGN outbursts must alter large-scale properties of the intracluster medium.

CONTENTS

INTRODUCTION TO X-RAY CLUSTERS OF GALAXIES 2
X-ray Emission from the Intracluster Plasma 3
Gas Temperatures and Masses 5
Mass Partitioning 6
Magnetic Fields 7
Transport Coefficients 7
Metal Abundances 8

CLASSICAL COOLING FLOWS 9
The Modern View of Cooling Flows 10

RADIO LOBE RELATED X-RAY STRUCTURE AND CAVITIES IN CLUSTER CORES . . . 12
Shock Fronts . . . 13
Ripples and Sound Waves . . . 15
Detectability of Cavity Systems . . . 15
Cavity Statistics . . . 16
Cavity Kinematics and Ages . . . 17
Stability of Cavities . . . 19
Radio Lobe Composition Inferred from X-Ray Observations of Cavities . . . 20
Radiative Efficiency of Radio Sources . . . 22
Simulations of Mixing by Radio Lobes . . . 22
Observations of Outflows and Mixing . . . 23

STABILIZING COOLING FLOWS BY FEEDBACK . . . 24
Heating and Cooling Rates in Clusters . . . 24
Heating and Cooling in Elliptical Galaxies and Groups . . . 26
Uncertainties in Estimating Jet Power . . . 27

HEATING MECHANISMS . . . 28
Cavity Heating . . . 28
Heating by Weak Shocks . . . 30
Heating by Sound Damping . . . 31
Cavity Enthalpy versus Shock Energy . . . 32
Distribution of AGN Heating within a Cluster . . . 33
Energy Injection by Radio Jets . . . 34

HEATING WITHOUT FEEDBACK . . . 35
Conduction . . . 35
Other Heating Mechanisms . . . 35

FEEDBACK AND GALAXY FORMATION . . . 36
Star Formation in cD Galaxies . . . 36
Galaxy Formation Models . . . 38
Supermassive Black Hole Growth as a Consequence of Feedback . . . 39
Accretion Mechanism . . . 40
Observational Constraints on Feedback Models . . . 40

CONCLUDING REMARKS . . . 41

1 INTRODUCTION TO X-RAY CLUSTERS OF GALAXIES

Clusters of galaxies are the largest gravitationally collapsed concentrations of matter in the Universe. With diameters of several megaparsecs and masses up to 10^{15} $M_\odot$, they are recognizable in photographs as distinct concentrations of galaxies centered on one or more brightest cluster members. The space between the galaxies is filled with a hot, dilute, plasma that emits X-rays and all is held in place by the gravity of a dark matter halo. The Perseus and Coma clusters were among the first clusters to be identified as X-ray sources by the Uhuru satellite in the early 1970s (Giacconi et al. 1971; Gursky et al. 1971; Forman et al. 1972). By the mid-1970s, at least 40 clusters of galaxies were identified as extended and powerful X-ray sources (Gursky & Schwartz 1977). A thermal origin for the X-ray emission was confirmed in the Perseus, Virgo, and Coma clusters with the detection of the collisionally excited, 6 – 7 keV Fe-K emission feature by the Ariel 5 (Mitchell et al. 1976) and OSO-8 observatories (Serlemitsos et al. 1977). Gas temperatures typically lie in the range of 10 million to 100 million K, cor-

responding to X-ray luminosities of $L_X \sim 10^{43}$ erg s^{-1} to 10^{45} erg s^{-1}. Roughly 90% of the baryons in clusters reside in the hot plasma, while the rest are locked up in stars in galaxies (Lin et al. 2003). The hot gas forms a hydrostatic atmosphere, where the temperature and density distributions reflect the gravitating mass. The atmosphere serves as a bank of baryons that failed to end up in stars and galaxies, and as a repository for the heat exhaust and detritus from stellar evolution and the growth of supermassive black holes during galaxy and cluster formation.

This review focuses on the latter, emphasizing new results from the Chandra and XMM-Newton X-ray Observatories showing that active galactic nuclei (AGN) lying at the hearts of galaxy clusters are pouring vast amounts of energy into the hot gas, some as prodigiously as quasars. The combination of high-resolution X-ray and radio imaging is yielding reliable measurements of this energy, which is apparently sufficient to suppress cooling flows and the substantial growth at late times of giant elliptical (gE) and cD galaxies. Deep Chandra images show that many clusters and gEs have multiple cavities, giving the hot atmospheres a Swiss-cheese-like topology that reveals the AGN outburst history independently of radio emission. These spectacular images are giving new insight into the particle and magnetic field content of radio sources, and are guiding the development of new radio jet and galaxy formation models. We discuss recent developments that link AGN outbursts to heating of the intracluster gas, and we tie these developments to several outstanding problems including the quenching of cooling flows, the exponential decline in the numbers of bright galaxies, the relationship between bulge mass and black hole mass in galaxies, and the possible contribution of AGN to excess entropy (preheating) in the hot atmospheres of groups and clusters. We briefly discuss some of the cosmological issues related to AGN heating in clusters. General reviews of clusters from an X-ray perspective were given recently by Mushotzky (2004) and Arnaud (2005), a review of clusters as cosmological probes was given by Voit (2005), and cold fronts and shocks associated with cluster mergers are reviewed by Markevitch & Vikhlinin (2007). We begin with a brief overview of the basic properties of clusters emphasizing the hot intracluster medium (ICM) and the scaling relations that describe it.

1.1 X-ray Emission from the Intracluster Plasma

The intracluster plasma (which we refer to interchangeably as hot gas) is composed primarily of ionized hydrogen and helium, mixed with traces of heavier elements, at roughly 1/3 of solar abundances. The presence of the gas can be understood in the context of hierarchical structure formation models. The warm baryons were swept inward with collapsing dark matter and subsequently heated to the virial temperature of the halo by accretion shocks and adiabatic compression. Mean gas temperatures of several tens to one hundred million Kelvin reflect the virial temperatures of halos, so that $T \propto \sigma^2$, where σ is the line-of-sight velocity dispersion of the cluster galaxies. Observed particle densities range from 10^{-4} cm^{-3} in the halos of clusters up to 10^{-2} cm^{-3} and higher in the centers of some clusters.

The gas can generally be treated as an optically thin coronal plasma in ionization equilibrium. The electrons and ions interact through Coulomb collisions and radiate mainly by thermal bremsstrahlung emission in the X-ray band (e.g., Sarazin 1988). At temperatures below 3×10^7 K, X-ray emission from the gas is

increasingly dominated by the recombination lines of iron, oxygen, silicon, and other elements (e.g., Sarazin 1988). The emission from heavy elements, particularly the iron K lines at 6 - 7 keV and the iron L lines below 1 keV in cooler plasmas, significantly alters the shape of the spectrum. This and the exponential decline in emission at high energies permit the temperature and metallicity of the hot gas to be measured accurately with modern X-ray telescopes.

The X-ray telescopes used to study clusters have commonly employed proportional counters or charge coupled devices (CCDs) as detectors. They are sensitive to photons with energies spanning the range 0.1 - 10 keV, well-matched to thermal radiation from the intracluster gas ($kT = 1$ keV for $T = 1.16 \times 10^7$ K). Because the emission processes are collisional, the power radiated per unit volume is proportional to the square of the density. X-ray surface brightness can therefore be used to determine gas density. With most X-ray instruments, for gas temperatures $kT \simeq 2$ keV or greater, the count rate from an optically thin thermal plasma depends almost exclusively on its emission measure, $\int n_{\rm e} n_{\rm H}\, dV$, where $n_{\rm e}$ is the electron number density, $n_{\rm H}$ is the equivalent hydrogen number density, and the integral is taken throughout the emitting volume. As a result, gas densities can be determined quite accurately, even when gas temperatures are poorly known.

The surface brightness of the hot gas declines with increasing radius, approximately as $I_{\rm X} \propto r^{-3}$ at large distances. Despite the rapid decline in surface brightness, the relatively low X-ray background permits X-ray emission to be traced to very large radii, making it an excellent probe of gas temperature, metallicity, and mass throughout much of the volume of a cluster.

Surface brightness profiles have traditionally been characterized using the isothermal "β-profile"

$$I_{\rm X} \propto [1 + (r/r_{\rm c})^2]^{-3\beta+1/2}, \tag{1}$$

where $r_{\rm c}$ is the core radius of the gas distribution, and the parameter $\beta \simeq 2/3$ for relaxed, bright clusters. As introduced (e.g., Cavaliere & Fusco-Femiano 1976; Branduardi-Raymont et al. 1981; Forman & Jones 1982), β is the ratio of the energy per unit mass in galaxies to that in the gas. However, this is an approximation that further relies on both the gas and dark matter being isothermal. This model provides a reasonably good fit to the surface brightness profiles of clusters at intermediate radii. In the central regions of some clusters, where the gas temperature declines and the density rises rapidly, the fit is poorer. At large radii, beyond roughly $0.3r_{200}$, the observed surface brightness profiles steepen below the β-profile (Vikhlinin et al. 2006). Here, r_{200} is the radius within which the mean mass density of the cluster exceeds 200 times the critical density of the Universe. For isothermal gas (or gas with $kT > 2$ keV), the β-model corresponds to the electron density profile

$$n_{\rm e}(r) = n_0[1 + (r/r_{\rm c})^2]^{-3\beta/2}, \tag{2}$$

where n_0 is the central electron density.

More generally, gas density and temperature profiles can be determined by "deprojection" (Fabian et al. 1981). Under the often inadequate assumption of spherical symmetry, the X-ray spectrum at any point in the cluster is determined in terms of simple integrals of temperature and density. Typically, the gas is represented as a number of shells of uniform density, temperature, and composition and its properties are determined by fitting X-ray spectra extracted from corresponding annular regions (Ettori 2000; Pointecouteau et al. 2004).

1.2 Gas Temperatures and Masses

The gas temperature of a hot atmosphere is most sensitive to the gravitating mass profile and, to a lesser degree, the history of heating by gravitational and nongravitational processes (Voit 2005; Babul et al. 2002). The connection between halo mass and gas temperature is clearly evident in the correlation between galaxy velocity dispersion and gas temperature (Edge & Stewart 1991). The scaling of this relationship is $\sigma \propto T^{0.63}$ in clusters with temperatures between 0.5 keV and 10 keV (e.g., Kochanek et al. 2003), which is close to the expected scaling $\sigma \propto T^{0.5}$. Simple theoretical models of gravitational collapse predict the present day scaling relationships between virial mass, X-ray gas temperature, and luminosity; $M \propto T^{3/2}$ and $L \propto T^2$ (Evrard et al. 1996). The observed scaling makes measured cluster temperatures and luminosities valued proxies for the much less accessible masses of dark matter halos. Departures from these scaling relations reflect physics beyond pure gravitational dynamics, including heating agents such as supernova explosions and AGN, and additional pressure support from magnetic fields and cosmic rays (Markevitch 1998; Voit 2005).

When the gas is spherically symmetric, in hydrostatic equilibrium, and only the thermal gas pressure is significant, the run of temperature and density with radius, in principle, permits the mass profile of clusters to be computed from the equation of hydrostatic equilibrium as

$$M(r) = -\frac{kTr}{G\mu m_{\rm H}} \left[\frac{d\log n_e}{d\log r} + \frac{d\log T}{d\log r} \right], \qquad (3)$$

where G is the gravitational constant, $m_{\rm H}$ is the hydrogen mass, and $\mu \simeq 0.61$ is the mean molecular weight of the ionized plasma. In practice, the logarithmic derivative of gas density is often evaluated using a parametrized model, such as the β-model, for the gas density, with the parameters determined by fitting the surface brightness profile. Similar methods can be applied to finding the logarithmic derivative of the temperature.

Mass determinations rely critically on the assumptions that the X-ray emitting gas is hydrostatic and the sole source of pressure. Other possible sources of pressure, including magnetic fields (Govoni & Feretti 2004), cosmic rays, and bulk motion of the gas, will cause masses to be underestimated. Velocity dispersion and weak lensing masses generally agree with X-ray masses to within a few tens of percent, except perhaps in systems undergoing major mergers. Simulations have shown that bulk motions cause the hydrostatic mass approximation to be biased below the true value by 5% to 20% (Nagai et al. 2007).

Vikhlinin et al. (2006) used Chandra observations extending to large radii to measure the mass versus temperature relationship for relaxed clusters with temperatures in the range of 0.7 – 9 keV. They found $M \propto T^{1.5-1.6}$, which agrees with self-similar models (Vikhlinin et al. 2006). There are disagreements between researchers about the normalization constant and temperature profile shapes, resulting in discrepancies in mass by a few tens of percent (e.g., Markevitch et al. 1998; Irwin & Bregman 2000; Allen et al. 2001; De Grandi & Molendi 2002; Vikhlinin et al. 2006). These discrepancies are often associated with the measurement of dT/dr at large radii, where systematic effects dominate. However, some of the scatter may be real and perhaps associated with accretion, mergers, or AGN-related activity.

The observed X-ray luminosity versus temperature relation for 3 – 10 keV

clusters scales as $L_{\rm X} \propto T^{2.6-2.8}$ which is steeper than expected for self-similar scaling ($\propto T^2$ Markevitch et al. 1998; Arnaud & Evrard 1999). The steepening is less significant in hot, relaxed clusters with gas temperatures above 5 keV (Allen et al. 2001), but becomes pronounced in cooler clusters and groups. This departure has been attributed to excess entropy or preheating of the gas prior to virialization. Likely energy sources are the same supernovae that enriched the gas with metals and AGN outflows from nascent supermassive black holes.

In the centers of clusters where radiative cooling is important, the gas temperature declines by factors of two to three (Allen et al. 2001; Vikhlinin et al. 2005). The temperature there reflects the reduction in $GM(r)/r$ over the central galaxy. It is in these so-called cooling flow regions where AGN outbursts are seen to have their biggest impact, as discussed below in detail.

1.3 Mass Partitioning

A galaxy cluster's gravitational influence extends over hundreds of cubic megaparsecs, which is enough in principle to capture a representative sample of the dark matter and baryons in the Universe. The form of the matter and its distribution throughout halos depends on both the history of galaxy formation and the cosmological parameters. X-ray and optical/IR observations show that the bulk of baryons reside in the hot ICM and that the fraction of baryons in stars decreases with cluster mass (the cold gas content is negligible). Only about 14% of the baryons in a 10^{14} $M_\odot$ cluster are in the stars, and this fraction decreases to 9% in 10^{13} $M_\odot$ clusters, possibly owing to a declining efficiency of galaxy formation with halo mass (Lin et al. 2003).

The gas mass fraction within r_{500}, the radius within which the mean mass density of a cluster exceeds 500 times the critical density of the Universe, depends weakly on gas temperature, rising to $\simeq 12\%$ in clusters hotter than ~ 4 keV (Vikhlinin et al. 2006). Gas mass fraction also varies with radius, and is affected by any process that modifies the amount of star formation or the energy content of the remaining gas, including radiative cooling and (pre-)heating (Kravtsov et al. 2005). The baryon fraction in clusters is the sum of the gas fraction and the stellar baryon fraction. Based on near-infrared luminosities of galaxies in clusters with masses of $\sim 3\times10^{14}$ $M_\odot$ (within r_{500}), the mass fraction in stars is approximately 1.64%. Therefore, the cluster baryon fraction within this radius is $\simeq 14\%$. This figure is close to the WMAP microwave background 3-year measurement (Spergel et al. 2007), which gives a Universal baryon fraction of 16% to 19%.

If the true baryon fraction is constant at a fixed radius in clusters and is constant over cosmic time (redshift), the dependence of the measured baryon fraction on luminosity distance can be a useful probe of the history of expansion of the Universe. Applying these assumptions to a study of 26 X-ray clusters extending to $z = 0.9$ with the Chandra observatory, Allen et al. (2004) found a high value for $\Omega_{\rm b}$ that is consistent with type 1a supernova and WMAP3 values. It must be emphasized that the assumptions that this technique relies on have not been shown to be valid. The baryon fraction is affected by the history of radiative cooling, feedback, and star formation, particularly in the cD, which are not well understood (Kravtsov et al. 2005).

1.4 Magnetic Fields

Faraday rotation measurements of background radio galaxies and radio galaxies within clusters have revealed that the intracluster gas is threaded with magnetic fields (Carilli & Taylor 2002; Kronberg 2003; Govoni & Feretti 2004; Vallée 2004). The Coma cluster's magnetic field was one of the first to be detected at a level of a few microgauss (e.g., Kronberg 2003). However, in the cores of cooling flow clusters (Section 2) field strengths of tens of microgauss have been inferred using Faraday rotation measures (Clarke et al. 2001). The ratio of magnetic pressure ($B^2/8\pi$) to gas pressure ($2n_{\rm e}kT$) is typically a few percent, so that magnetic fields are dynamically unimportant in clusters, except occasionally in the inner several kiloparsecs or so. Magnetic fields may have been deposited by radio galaxies and or quasars, or they may be primordial fields that have been amplified over time by gas turbulence and/or compression (Carilli & Taylor 2002).

1.5 Transport Coefficients

Magnetic fields can modify the transport coefficients significantly because the ratio of the Coulomb mean free path to the Larmor radius of a thermal proton is $\simeq 10^8 B(kT)^{3/2} n_{\rm e}^{-1}$, where the magnetic field, B, is in μG, the temperature, kT, is in keV, and $n_{\rm e}$ is the electron density in cm^{-3}. The same ratio for electrons is a factor of $\sqrt{m_{\rm p}/m_{\rm e}}$ larger, so that electrons and ions are both tied rigidly to magnetic field lines for typical values of the intracluster magnetic field (e.g., Govoni 2006). One might then expect thermal conduction and viscous forces to be controlled entirely by the structure of the magnetic field (e.g., Tribble 1989). However, under similar conditions in the solar wind, thermal conduction appears to be suppressed by only a modest factor and it has been argued that this should be true generally for turbulent plasmas (e.g., Sarazin 1988; Rosner & Tucker 1989; Narayan & Medvedev 2001).

Many empirical arguments favor greater suppression of thermal conduction in clusters. A number of researchers argue that thermal conduction must be suppressed from the Braginskii value for a nonmagnetized plasma (Spitzer 1962; Braginskii 1965) by factors of up to 1000 or more in order to have sharply defined "cold fronts" (Ettori & Fabian 2000; Kempner et al. 2002). Vikhlinin et al. (2001b) argue that cold fronts are a special case, because shear can amplify magnetic field parallel to the front, effectively suppressing heat flow across the front. For example, they conclude that a ~ 10 μG field is required in the cold front in Abell 3667 to explain suppression of Kelvin-Helmholtz instability, although Churazov & Inogamov (2004) point out that curvature suppresses growth of the instability, significantly weakening this conclusion.

As another example, Vikhlinin et al. (2001a) found ~ 3 kpc remnants of the interstellar medium in NGC 4874 and NGC 4889 at the center of the Coma cluster. In order for these to survive thermal evaporation, they found that thermal conduction must be suppressed there by a factor of 30 - 100 from the Braginskii value. Again, these are special cases which may not be representative of the general ICM. However, Markevitch et al. (2003) argue that temperature variations in Abell 754 require thermal conductivity to be suppressed by at least an order of magnitude. Their result is determined for 100 kpc scale regions throughout the cluster that are not associated with any special structures.

There are fewer limits on the viscosity. Based on the morphology of Hα fil-

aments near the northwestern ghost cavity in the Perseus Cluster, Fabian et al. (2003b) argue that the flow there is laminar, hence that the viscosity is suppressed by a factor of no more than 15. This interpretation is supported by numerical simulations (Reynolds et al. 2005). With electrons and protons both tied so tightly to the magnetic field lines, it is reasonable to expect similar levels of suppression for thermal conductivity and viscosity. Taken together, the observational limits suggest suppression of thermal conduction by somewhat more than expected from theory and observations of the solar wind and, perhaps, a similar level of suppression of viscosity. The constraints are showing signs of converging, but there is no consensus. Unsatisfactory though it is, transport coefficients in the hot ICM are not well determined.

1.6 Metal Abundances

The intracluster plasma is enriched with heavy elements to an average metallicity of roughly 1/3 of the solar value (Arnaud et al. 1992), which is roughly the universal average mean metal abundance (Renzini 2004). Elements heavier than helium are created by stellar evolution, particularly by core collapse supernova explosions of massive stars (SNe II), and by thermonuclear detonations of accreting white dwarf stars (SNe Ia), which also play a significant role in their dispersal. Core collapse supernovae presumably seeded the Universe with metals during the early stages of galaxy formation, while SNe Ia, which are associated with the late stages of stellar evolution of less massive stars, dominate metal production over longer time spans. Clusters of galaxies are close to being "closed boxes" and thus retain the memory of metal enrichment through star formation and stellar evolution. SNe Ia are major producers of iron, whereas SNe II produce high yields of the alpha elements (Si, S, Ne, Mg). X-ray measurements of the relative abundance of the metallic species are thus able to constrain the history of star formation.

The iron mass in the hot gas in clusters correlates with the luminosity of the elliptical and lenticular galaxy population but not with the luminosity of spirals. Moreover, alpha element abundances relative to iron in hot clusters are inconsistent with those in the Milky Way (Baumgartner et al. 2005). Therefore, most of the heavy elements were created by stars bound to the early-type galaxies (Arnaud et al. 1992). The iron mass in the gas exceeds the iron mass in stars in galaxies by at least a factor of two (Arnaud et al. 1992; Renzini 2004), implying that cluster galaxies have ejected most of the metals they produced over cosmic time. If the iron in the ICM was shed by the stars, then the ratio of the iron mass to total stellar mass in clusters is a factor of four larger than expected for a population of stars like those in the Milky Way (Lowenstein 2006), implying that star formation as it proceeds in the Milky Way would have difficulty producing the observed levels of iron in clusters. It is unlikely that SNe Ia could have supplied most of the iron unless the supernova rate was much higher in the past. Furthermore, SNe II underproduce iron by a factor of five if galaxies formed with a Salpeter initial mass function (IMF). It appears that most of the iron was produced by SNe II in a rapid phase of early star formation that proceeded with an IMF heavily weighted toward massive stars relative to the IMF operating in present day spiral galaxies (Renzini 2004; Lowenstein 2006). No evidence has been found for strong changes in abundance with lookback time out to $z \sim 0.5$, which is consistent with early enrichment scenarios (Mushotzky & Loewenstein

1997).

Abundance gradients corresponding to average metallicity increases of factors of two or more are routinely found in the central ~ 100 kpc regions of cD clusters (Ezawa et al. 1997; Ikebe et al. 1997; Finoguenov et al. 2000; De Grandi & Molendi 2001; Irwin & Bregman 2001). High-resolution Chandra studies have shown that the gradients are strongest near the cD and that they sometimes track the stellar isophotes (Wise et al. 2004). For example, in Hydra A, (David et al. 2001) found that the iron abundance rises from 30% of the solar value at 100 kpc to about 60% in the nucleus of the cD, and that the silicon abundance rises from roughly half the solar value to the solar value in the nucleus. They attribute the gradient to constant SNe Ia production from the central galaxy over the past several gigayears. A similar situation is found in M87 (Finoguenov et al. 2002), where most of the iron seems to have originated from SNe Ia, while only 10% was injected from SNe II. Intriguingly, Tamura et al. (2004) found that SNe II enrichment from massive star formation may be important in the cores of some clusters. Star formation is often observed in cD galaxies centered in cooling flows, which could contribute significantly to the gradients.

2 CLASSICAL COOLING FLOWS

A cooling flow cluster is characterized by bright X-ray emission from cool, dense gas in the central region of the cluster (see Fabian 1994 for a more comprehensive review of the basic operating principles of a cooling flow). Within the cooling radius, where the cooling time of the gas is less than the time since the last major heating event, the surface brightness of the gas near a central cD galaxy often rises dramatically above a β-model, by factors of up to 100, corresponding to a rise in gas density by factors of 10 or more. The X-ray luminosity within the cooling region reaches values of 10^{45} erg s^{-1} in the extreme. In many cases it is more than 10% of the cluster's total luminosity. If this luminosity is uncompensated by heating, the gas will radiate away its thermal and gravitational energy on a timescale of $t_{\rm cool} = p/[(\gamma-1)n_{\rm e}n_{\rm H}\Lambda(T)] < 10^9$ year (Silk 1976; Cowie & Binney 1977; Fabian & Nulsen 1977; Mathews & Bregman 1978), where p is the gas pressure, $\Lambda(T)$ is the cooling function, and γ is the ratio of specific heats of the gas. As the gas radiates, its entropy decreases and it is compressed by the surrounding gas, causing it to flow inward. The cooling time decreases as the gas density increases and, eventually, the gas temperature drops rapidly to $< 10^4$ K, so that cooled gas condenses onto the central galaxy. The condensing gas is replenished by hot gas lying above, leading to a steady, long-lived, pressure-driven inward flow of gas at a rate of up to 1000 M$_\odot$ year^{-1} (Fabian 1994).

Observed cooling times are significantly longer than free-fall times, so that the gas remains very nearly hydrostatic as it cools. The flow is then governed by cooling, making the flow time $t_{\rm flow} = r/v$, where v is the radial speed of inflow, approximately equal to the cooling time. Counterintuitively, the heat lost to radiation does not necessarily make the gas temperature decrease. The inexorable entropy decrease is offset by adiabatic compression as gas flows inward, so that, typically, the temperature of the cooling gas follows the underlying gravitational potential, i.e., $kT/(\mu m_{\rm H})$ is a multiple of order unity of the "local virial temperature," $GM(r)/r$ (e.g., solutions of Nulsen 1986 with $k = 0$). Cooling gas would therefore remain approximately isothermal in an underlying isothermal

potential. Because the virial temperature of cluster central galaxies (revealed by their stellar velocity dispersions) is typically lower than that of the surrounding cluster, the gas temperature declines inward in a classical cooling flow. Rather than being a direct manifestation of cooling, this temperature drop reveals the flattening of the underlying gravitational potential. (If gas cools enough to flow inward, this feature will persist in more up-to-date cooling flow models.) The Mach number of the flow increases inward, until it approaches unity. Up to that point, linear growth of the thermal instability is suppressed by buoyant motions (Balbus & Soker 1989), but beyond it cooling is too fast and the gas is expected to form a rain of thermally unstable clouds that cool rapidly to low temperature.

The classical cooling flow is approximately steady within the region where the cooling time is shorter than its age. The power radiated from the steady flow equals the sum of the enthalpy carried into it and the gravitational energy dissipated within it. To a first approximation, the gravitational energy can be ignored, so that the luminosity $L_{\rm X} \simeq \dot{M}(5kT)/(2\mu m_{\rm H}) \simeq 1.3 \times 10^{44} T_5 \dot{M}_2 2$ erg s^{-1}, where the temperature of the gas entering the flow is given by $T_5 = (kT/5$ keV) and the cooling rate is given by $M_2 = \dot{M}/(100$ M$_\odot$ year^{-1}). This expression is exact for steady, isobaric cooling.

This single-phase cooling model predicts central spikes in surface brightness that are clearly stronger than observed, a discrepancy that prompted the introduction of inhomogenous cooling flow models. Such models postulate a broad spectrum of gas temperature and density at each radius (Nulsen 1986). Both Rayleigh-Taylor and shear instabilities can disrupt an overdense cloud if the distance it must move to reach its convective equilibrium position exceeds its size (alternatively, if its fractional overdensity is greater than its size divided by the distance to the cluster center). Such nonlinear overdensities therefore tend to be shredded finely, slowing their motion relative to the bulk flow and enabling them to be pinned to the flow by small stresses (e.g., magnetic stresses). Tying overdensities to the bulk flow then permits the growth of thermal instabilities throughout the core of the cluster, leading to widespread deposition of cooled parcels of gas and making the mass flow rate, $\dot{M}$, a strong function of the radius. This solution avoids the need for strong X-ray and UV surface brightness spikes centered on the cD's nucleus by distributing the hundreds of solar masses of gas and star formation deposited each year throughout the cooling region of the cluster.

This cooling flow model has been under siege for years, primarily because of its failure to predict the observed amount and spatial distribution of star formation, line emission, and other expected products of cooling, which are generally observed only in the inner few tens of kiloparsecs. The spatial distribution of cool gas and star formation is more consistent with the single-phase model, but at levels that fall orders of magnitude below the predictions. This failure implies that the gas is not condensing at the predicted rates, and that radiation losses are either being replenished, or the gas is condensing into an unseen state. Sensitive searches for the repository in optical, infrared, and radio bands have severely restricted the latter possibility, if not ruled it out entirely.

2.1 The Modern View of Cooling Flows

The strongest spectroscopic signatures of cooling gas are X-ray emission lines below 1 keV of various charge states of Fe L (Böhringer et al. 2002). Early ob-

servations of M87 and a few other bright clusters made with the Einstein Observatory's Focal Plane Crystal Spectrometer [FPCS](Canizares et al. 1982, 1988) apparently detected these Fe L lines at the 4σ to 6σ level. Remarkably, the line strengths from gas at temperatures of a few million to a few tens of million degrees agreed with predictions of the classical cooling flow model. Unfortunately, the FPCS, with an effective area of only one square centimeter, was unable to achieve detections of higher statistical significance. Nevertheless, for two decades these concordant results were bolstered by signatures of cooling at other wavelengths: filaments of Hα emission from warm, ionized gas (Heckman 1981); star formation (Johnstone et al. 1987; McNamara & O'Connell 1989); and pools of cold atomic and molecular gas (Edge 2001) provided support for a classical cooling flow model, albeit at lower rates.

The situation changed dramatically when far more sensitive XMM-Newton Reflection Grating Spectrometer (RGS) observations failed to confirm the picket fence of lines, including the Fe L features, at ~ 1 keV from cooling gas in spectra of the clusters Abell 1835 (Peterson et al. 2001) and Abell 1795 (Tamura et al. 2001). The prominent and useful Fe XVII line at 12 Å is either weak or absent in cooling flow clusters (Peterson et al. 2003), although there is a hint of Fe XVII emission in the Abell 2597 cluster at a level that is consistent with a cooling rate of ~ 100 $M_\odot$ year^{-1} (Morris & Fabian 2005). Ultraviolet line emission also suggests cooling rates about an order of magnitude smaller than previous estimates (Oegerle et al. 2001; Bregman et al. 2006).

The relationship between cooling rate and line power that is central to this issue was first noted by Cowie (1981). In terms of the entropy, S, the energy equation of cooling gas is $\rho T dS/dt = -n_e n_H \Lambda(T)$, where ρ is the gas density, t is the time and other terms are as above. Rearranging this to describe a fluid element in gas cooling steadily at the rate $\dot{M}$ gives the mass of the element as $dM = \dot{M}\,dt = -\dot{M}\rho T dS/[n_e n_H \Lambda] = \rho\,dV$, where dV is its volume, so that the emission measure of the element is $n_e n_H\,dV = -\dot{M} T dS/\Lambda$ (where $dS < 0$ for cooling gas). In terms of the pressure and temperature, $dS = [\gamma\,dT/(\gamma-1)T - dp/p]k/(\mu m_H)$. As the gas cools and flows inward, its pressure generally increases, so that $-dS$ is minimized for isobaric cooling ($dp = 0$ and $dT < 0$; late stages of cooling can be isochoric, reducing the integrand below by a factor of γ at sufficiently low temperatures). If the contribution of a line (or group of lines) to the cooling function is $\Lambda_{line}(T)$, then the total power radiated in that line by gas cooling isobarically in a steady flow is

$$P_{line} = \int n_e n_H \Lambda_{line}(T)\,dV = \dot{M}\frac{\gamma}{\gamma-1}\frac{k}{\mu m_H}\int_0^{T_i}\frac{\Lambda_{line}(T)}{\Lambda(T)}\,dT,$$

where T_i is the temperature that the gas cools from (the sense of integration has been reversed here). If the gas pressure increases as the gas cools, the power radiated in the line would be greater and this expression would overestimate the cooling rate.

The failure to detect the low energy X-ray lines at the expected levels indicates that the canonical cooling rates were overestimated by an order of magnitude or more, although the picture is not so simple (Peterson & Fabian 2006). In the classical cooling flow model, thermally unstable gas clouds are expected to be approximately isobaric, so that the constant pressure cooling model should be reasonably accurate, especially for lines emitted mainly by gas that is cooler than average. As outlined above, the constant pressure cooling model makes spe-

cific predictions of the strengths of lines from low temperature cooling gas (cf. Böhringer et al. 2002; Peterson & Fabian 2006). These predictions are inconsistent with the line strengths observed by Peterson et al. (2003), which require the emission measure to decrease more rapidly with temperature than expected for the constant pressure cooling flow model. This behavior cannot be explained by merely reducing the cooling rate.

The absence of multiphase gas is confirmed in moderate spectral resolution CCD data from Chandra, XMM-Newton, and ASCA. In general, the deprojected gas profiles in cooling flows can be adequately modeled by a single temperature plasma at each radius (McNamara et al. 2000; David et al. 2001; Molendi & Pizzolato 2001), except perhaps near the nucleus of the cD, where star formation is frequently observed.

It may be possible for nonradiative cooling to proceed at or near the canonical rates without revealing X-ray line emission. Processes such as gas-phase mixing, differential photoelectric absorption, and rapidly cooling, unresolved, high metallicity inclusions in the hot gas (Fabian et al. 2001) are possible. If so, the problem of identifying the permanent repository for the cooling material would remain.

3 RADIO LOBE RELATED X-RAY STRUCTURE AND CAVITIES IN CLUSTER CORES

Disturbances in the hot gas near NGC 1275 were first noted in an early Einstein Observatory image of the Perseus cluster (Branduardi-Raymont et al. 1981; Fabian et al. 1981). A decade later, Rosat's 5 arcsec High Resolution Imager (HRI) associated the disturbances with two cavities filled with radio emission emanating from the nucleus of NGC 1275 (Böhringer et al. 1993). Similar disturbances were later noted in HRI images of other bright cD clusters (e.g., Carilli et al. 1994; Huang & Sarazin 1998; Owen & Eilek 1998; Rizza et al. 2000), but limitations in Rosat's spatial and spectral resolution stalled any further progress on the nature and import of these disturbances until the launches of Chandra and XMM-Newton in 1999.

We now know that nearly three dozen cD clusters and a similar number of gE galaxies and groups harbor cavities or bubbles in their X-ray halos (Fabian et al. 2000; McNamara et al. 2000, 2001; Schindler et al. 2001; Heinz et al. 2002; Mazzotta et al. 2002). Cavity systems are difficult to detect, so this is surely a lower limit to their numbers. Like the radio lobes that created them, cavities are usually found in pairs of approximately elliptical X-ray surface brightness depressions, 20% to 40% below the level of the surrounding gas. This is the expected decrement toward a spheroidal empty cavity embedded in a β-model atmosphere (Fabian et al. 2000; McNamara et al. 2000; Blanton et al. 2001, 2003; Nulsen et al. 2002). Cavity systems in clusters vary enormously in size, from diameters smaller than 1 kpc like those in M87 (Forman et al. 2005, 2007) to diameters approaching 200 kpc in the MS0735.6+7421 and Hydra A clusters (McNamara et al. 2005; Nulsen et al. 2005b; Wise et al. 2007). A correlation exists between radio luminosity and cavity power (Section 5.1; e.g., Bîrzan et al. 2004; Dunn & Fabian 2006), but with a large scatter that is poorly understood.

One of Chandra's early surprises was the discovery of cavities devoid of bright 1.4 GHz radio emission. They were dubbed ghost cavities, and were interpreted

as aging radio relics that had broken free from the jets and had risen $20-30$ kpc into the atmosphere of the cluster (McNamara et al. 2001; Fabian et al. 2002). We now know they are filled with low-frequency radio emission and may be connected by tunnels back to the nucleus (Clarke et al. 2005; Wise et al. 2007). Some clusters have multiple pairs of cavities, apparently produced by multiple radio outbursts or quasicontinuous outflows.

The work required to inflate the cavities against the surrounding pressure is roughly $pV \sim 10^{55}$ erg in gEs (e.g., Finoguenov & Jones 2001) and upward of $pV = 10^{61}$ erg in rich clusters (e.g., Rafferty et al. 2006). The total energy needed to create a cavity is the sum of its internal (thermal) energy, E, and the work required to inflate it, i.e., its enthalpy, $H = E + pV$. This is several times pV. The displaced gas mass is several 10^{10} $M_\odot$ in an average cluster system such as Abell 2052 (e.g., Blanton et al. 2001) but can exceed 10^{12} $M_\odot$ in powerful outbursts such as those in MS0735.6+7421 and Hydra A. The cavities in these systems occupy between 5% and 10% of the volume within 300 kpc giving the hot ICM a Swiss cheese-like topology (Wise et al. 2007). The bright rims or shells surrounding many cavities are cooler than the ambient gas (Fabian et al. 2000; McNamara et al. 2000; Blanton et al. 2001, 2003; Nulsen et al. 2002) and thus are not active shocks as anticipated in early models (e.g., Heinz, Reynolds, & Begelman 1998). Evidently, the cavities are close to being in pressure balance with the surrounding gas. A nearly empty cavity will rise into the cluster atmosphere like a buoyant weather balloon, traveling at a speed approaching the local free-fall velocity. The cool rims are probably composed of displaced gas dragged outward from the center by the buoyant cavities (Blanton et al. 2001; Churazov et al. 2001; Reynolds et al. 2001).

Cavity systems are often surrounded by belts (Smith et al. 2002), arms (Young et al. 2002; Forman et al. 2005, 2007), filaments, sheets (Fabian et al. 2006), and fragile tendrils of gas maintained against thermal evaporation, perhaps, by magnetic fields threaded along their lengths (Nipoti & Binney 2004; Forman et al. 2007). This structure is usually composed of cooler gas and is associated with H emission that may be tracing circulation driven by rising radio lobes and cavities (Fabian et al. 2003b). "Swirls" of cool X-ray gas were found in the central regions of the Perseus (Fabian et al. 2006) and Abell 2029 (Clarke et al. 2004) clusters, which may be related to merger activity or circulation flows generated by radio sources (e.g., Mathews & Brighenti 2003; Heinz et al. 2006). At present, this wealth of structure is not well understood.

Owing to their proximity and high surface brightnesses, the M87 and Perseus clusters are spectacular exemplars of these structures (Figure 1). Keep in mind, however, that neither is outstanding in its power output. The AGN (cavity) power in Perseus is about 25 times larger than that of M87, and Perseus itself is feeble compared to Cygnus A and MS0735.6+7421, which are roughly 215 and 270 times, respectively, more energetic than Perseus (Rafferty et al. 2006). Some 18 of the 33 cavity systems studied by Rafferty et al. (2006) exceed the AGN power output of Perseus, suggesting the Perseus and Virgo clusters serve as useful benchmarks for average to low power outbursts.

3.1 Shock Fronts

With the notable exceptions of the Mach 8 shock in Centaurus A (Kraft et al. 2003), the Mach 4 shock in NGC 3801 (Croston et al. 2007), and perhas sur-

rounding the overpressured quasar 3C186 (Siemiginowska et al. 2005) there is little evidence for strong shocks surrounding the radio-lobe cavities studied with Chandra. However, evidence of weaker, more remote shocks is accumulating. Jones et al. (2002) reported gas features near NGC 4636 consistent with a Mach 1.7 shock. Smith et al. (2002) saw evidence of shocks around the radio source Cygnus A. More recently, Chandra images of clusters have revealed roughly elliptical breaks in surface brightness enveloping the inner radio-lobes of M87 (Forman et al. 2005) and the enormous cavity systems in MS0735+7421 (Figure 2), Hydra A, and Hercules A (McNamara et al. 2005; Nulsen et al. 2005a,b). These structures resemble the classical cocoon shocks thought to envelope powerful radio sources as they advance into the surrounding medium. Modeled as a spherical shock from a nuclear outburst, the surface brightness discontinuities can be reproduced by conventional shock waves with Mach numbers lying between 1.2 and 1.7 (McNamara et al. 2005; Nulsen et al. 2005a,b). Though the shocks are only mildly supersonic (weak) they can encompass huge volumes, $200 - 400$ kpc in radius and require energy deposition upward of 10^{61} erg into the intracluster gas. The shock energy corresponds to several pV per cavity, comparable to the free energy of the cavities themselves (see also Wise et al. 2007). Thus the cavity enthalpy provides only a lower limit to the total outburst power. The ages of these outbursts, estimated from shock models (approximately the shock radius divided by the shock speed), are reassuringly similar to buoyant rise times of their cavities, although significant differences found, for example, in Hydra A are related to the outburst history and the partitioning of energy between enthalpy and shock heating (Section 3.5).

Detecting the expected gas temperature rises behind these shock fronts has proved difficult. Radiative losses are negligible on timescales of interest, so that shocks in the ICM should conserve energy. Furthermore, the magnetic field in the bulk of the ICM is dynamically insignificant and does not affect shocks significantly for pure magnetohydrodynamic shocks (e.g., Nulsen et al. 2002). Some shock energy can be absorbed by particle acceleration, but this is expected to be small for weak shocks. Under these conditions, the ICM should be well approximated as an ideal gas with a constant ratio of specific heats, $\gamma = 5/3$, leading to the well-defined relationship,

$$\frac{T_2}{T_1} = \frac{(\gamma+1)\rho_2/\rho_1 - (\gamma-1)}{[(\gamma+1) - (\gamma-1)\rho_2/\rho_1]\rho_2/\rho_1}, \tag{4}$$

between the shock temperature jump, T_2/T_1, and density jump, ρ_2/ρ_1. For example, for the Mach 1.2 shocks in Hydra A and M87 the temperature jumps by 20% behind the shock. However, the temperature declines rapidly behind the shock because of adiabatic expansion. When projected onto the sky, emission from the shocked gas is also diluted by emission from the surrounding unshocked gas. As a result, the projected emission-weighted temperature has a peak rise of only 5%. Given that thousands of photons are required to measure temperatures accurately, few such temperature rises have been detected. Examples of detections include the 14 kpc ring in M87 (Forman et al. 2007), MS0735.6+7421 (McNamara et al. 2005), Hercules A (PEJ Nulsen, in preparation), Centaurus A (Kraft et al. 2003), and NGC 4552 (Machachek et al. 2006).

For MS0735.6+7421 and Hercules A, the mean jet power released into the ICM over $\sim 10^8$ years is more than 10^{46} erg s^{-1}, which is comparable to a powerful quasar. The bulk of this energy is deposited beyond the cooling region of those

clusters. Despite this quasar-like power, the cD hosts share few quasar characteristics (e.g., broad nuclear emission lines), although this issue needs further study. The energy deposited in the inner 1 Mpc of MS0735.6+7421 corresponds to a few tenths of a keV per particle, which is a significant fraction of the $\sim$ 1 keV required to supply the excess entropy (preheating) in clusters (Wu et al. 2000; Roychowdhury et al. 2004; Voit & Donahue 2005). Thus several outbursts of this magnitude during the life of a cluster, particularly in the early stages of its development, could preheat it (see Section 1.2). No clear distinguishing characteristics have yet been noted between the cD galaxies hosting powerful outbursts and cDs in other cooling flows. Thus occasional powerful outbursts, if they occur in all systems, could dominate the energy output from smaller, more frequent outbursts integrated over cluster ages.

Voit & Donahue (2005) have identified several clusters with strongly boosted central entropy profiles and relatively weak radio sources that otherwise show no evidence of recent AGN activity. They suggested that the central entropy boosts were imprinted by shocks generated by powerful AGN outbursts that occurred in the past, although the AGN are dormant at present. Furthermore, Voit & Donahue found that the entropy profiles are generally consistent with shock heating in the inner few tens of kpc, but the mode of heating switches to cavities and sound waves further out. An additional consequence of repeated powerful outburts is the substantial growth at late times of the black holes at the core of the AGN, which is discussed further in Section 7.2.

Luminosity boosts, gas clumping, and gas outflows caused by AGN outbursts could, in principle, affect measurements of cosmologically important quantities such as gas mass fractions, the luminosity function, and cluster masses. However, these effects are likely to be subtle and are just beginning to be explored (e.g., Kravtsov et al. 2005; Gitti et al. 2007).

3.2 Ripples and Sound Waves

The best known example of weak shocks or sound waves is that in the Perseus cluster. It is seen as a spectacular system of ripples and other disturbances in an 890 ksec Chandra image (Fabian et al. 2006). The half dozen ripples lying beyond the inner cavity system (Figure 1) are separated by roughly 11 kpc and are visible out to a radius of 50 kpc (Fabian et al. 2003a). The ripples appear to be pressure disturbances with amplitudes of 5% to 10%, or sound waves (weak shocks) propagating outward with a period of $\sim 10^7$ year (Fabian et al. 2003a, 2006). Apparently the gas within 25 kpc surrounding the cavity system is overpressured by about 30%, implying that the entire inner halo is expanding. Cavity pV work alone would then underestimate the AGN power in Perseus. Temperature jumps across the ripples and the band of high pressure have not been found, despite the ample number (70 million) of detected photons available. Fabian et al. (2006) have suggested that thermal conduction is suppressing the temperature jumps by creating isothermal shocks. This phenomenon is poorly understood.

3.3 Detectability of Cavity Systems

Studies of cavity populations should in principle yield information on the AGN duty cycle, the energy per AGN outburst, and outburst ages, once a reliable dynamical model has been established and the complicating issues of cavity de-

tectability, stability, and lifetime are understood. In a genuinely random sample of galaxy clusters, radio jets and their associated cavities are expected to emerge from the cD's nucleus at random orientations with respect to the plane of the sky. The decrement in surface brightness of a cavity relative to the surrounding cluster, i.e., its detectability, will be a strong function of its size and distance from the cluster center, as well as its aspect with respect to the plane of the sky. In the simplest approximation, a small bubble of radius r on the plane of the sky at a distance R from the cluster center produces a count deficit (cavity) scaling as $r^3(1+R^2/a^2)^{-3\beta}$, where β and a are the β-model parameters for the cluster. The cluster count from over the bubble scales as $r^2(1+R^2/a^2)^{-3\beta+1/2}$ and the noise in this scales as its square root. Thus the signal-to-noise ratio scales as $r^2(1+R^2/a^2)^{-3\beta/2-1/4}$, implying that cavities are easiest to detect when they are large and are located in the bright central regions of the cluster. This simple argument does not take projection into account, but should apply roughly to bubbles within 45° of the plane of the sky as seen from the cluster center. Bubbles far from the plane of the sky are difficult to detect at any radius.

The detectability of a cavity system as a function of its age and nuclear distance (time) was modeled by Enßlin & Heinz (2002), who considered spherical bubbles of adiabatic, relativistic plasma embedded in an isothermal cluster with a core radius $r_{\rm c} = 20$ kpc. As a cavity rises, it expands adiabatically from its initial volume, V_0, to a modestly larger volume, V_1, at its observed location as $V_1 = V_0(p_0/p_1)^{1/\Gamma}$, where p_0 and p_1 are the ambient pressures at the respective locations, and Γ is the ratio of specific heats within the cavity. For a spherical cavity, the ratio of its radius, r, to the distance, R, from the cluster center therefore evolves as

$$\frac{r}{R} = \frac{r_0}{R_0}\left(\frac{R}{R_0}\right)^{-1}\left[\frac{p(R)}{p(R_0)}\right]^{-1/(3\Gamma)}, \qquad (5)$$

where $p(R)$ is the pressure of the ICM at distance R and subscripts "0" denote initial values. Enßlin & Heinz found that the contrast of a cavity launched from the center of the cluster along the plane of the sky is a slowly decreasing linear function of distance, until the cavity vanishes into the background at large distances. The detectability of cavities rising at oblique angles with respect to the plane of the sky declines according to a power law with distance. From figure 3 of Enßlin & Heinz (2002), we find that the detectability declines $\propto R^{-1}$ and $\propto R^{-2.5}$ for cavities launched at 45° and 90°, respectively, from the plane of the sky. These estimates do not include the effects of cavity rims, which enhance cavity contrast, nor of cavity disruption (Section 3.6), that works in the opposite direction. Nevertheless, they imply that once cavities have ventured distances of several times their initial radii, their chances of detection decline rapidly.

3.4 Cavity Statistics

The statistical properties of cluster cavities drawn from the Chandra archive, together with their attendant radio sources, have been studied in some detail (e.g., Bîrzan et al. 2004; Dunn & Fabian 2004, 2006; Dunn et al. 2005; Rafferty et al. 2006). These studies are hobbled by unknown selection effects in the Chandra archive. Nevertheless, they suggest a high incidence of detectable cavity systems in clusters, groups, and galaxies, spanning a large range of gas temperature. The detection frequencies found in the samples of Bîrzan et al. (2004) and

Rafferty et al. (2006) are 20% (16/80) and 25% (33/130), respectively. Using the flux-limited sample of the brightest 55 clusters observed by the Rosat observatory (Peres et al. 1998), Dunn et al. (2005) found between 12 and 15 clusters with cavity systems, giving an overall detection rate of between 22% and 27%. Their detection rate rose to 70% (12/17) in strong cooling flows (Dunn et al. 2005). The detection rate is close to 25% (27/109) for a sample of nearby gEs with significant hot atmospheres (Nulsen et al. 2007). While there is considerable overlap between the three cluster samples, the gE sample is largely independent (Section 4.3).

The Rafferty et al. (2006) sample is the most extensive cluster sample available, and thus provides a good representation of average cavity properties in clusters. The distribution of projected distances between the nucleus of the host cD and cavity centroid in Figure 3 shows that the detection rate peaks in the inner 30 kpc or so and declines rapidly at larger distances. Only the rarest and most powerful outbursts produce detectable cavities beyond $\sim$ 100 kpc. Within 100 kpc the detection frequency declines formally as $\sim R^{-1.3}$, but is consistent with $\sim R^{-1}$, the expected rate of decline for cavities launched on random trajectories (Section 3.3).

The distribution of observed cavity sizes (Figure 4) shows a typical value of 10 – 15 kpc in radius with no preferred size. The distribution of the ratio of projected nuclear distance to radius, shown in Figure 5, peaks at $R/r \simeq 2$ and falls off rapidly beyond. Evidently, cavities travel roughly their own diameters before they disintegrate or become too difficult to detect. Other than the most powerful systems, cavities are found within the light of the central galaxy. The distribution of buoyancy ages (Figure 6) shows a typical age of $\sim 10^7$ years but some are greater than $\sim 10^8$ year.

The difficulty of detecting cavities coupled with the highly variable image quality (depth) of the Chandra archive suggest that the existing inventory of cavities is incomplete. Most, if not all, cooling flow clusters probably harbor cavity systems or have done so in the recent past.

3.5 Cavity Kinematics and Ages

During its initial stages, the tip of a radio jet advances supersonically into the surrounding medium (e.g., Scheuer 1974; Gull & Northover 1973; Blandford & Rees 1974; Heinz, Reynolds, & Begelman 1998; Enßlin & Heinz 2002). As the ram pressure of the jet declines with respect to the ambient pressure, it decelerates, eventually shuts down, and the radio lobes quickly reach pressure balance with the surrounding hot ICM (Begelman 2004). During the initial, supersonic stage, the cavity created by the tip of a jet can be long and narrow. Only ICM near the advancing jet tip is subjected to the strongest shocks, and relatively little of the X-ray emitting gas within the region encompassed by the jet is shocked. A narrow cavity produces a small deficit in the X-ray emission, making it difficult to detect. Enhanced X-ray emission from the relatively small volume of shocked gas may not stand out when superimposed on the general cluster emission. In order to form the roughly spherical cavities that are observed, the expansion of a cavity has to "catch up" with the jet tip, so that the cavity displaces a much greater proportion of the X-ray emitting gas within the extent of the jets. This may come about when the pressure within a radio lobe becomes comparable to the ram pressure of the jet, so that the lobe expands into the surrounding gas at

a speed similar to the tip of the jet, or because the jet wanders enough to carve out a large cavity (e.g., Heinz et al. 2006). At formation, such a cavity can have an age that is appreciably shorter than its sound crossing time and a lot less than its buoyant rise time.

A cavity is buoyed outward with a force, $F_{\rm b} = Vg(\rho_{\rm a} - \rho_{\rm b})$, where V is its volume, g is the local gravitational acceleration, $\rho_{\rm a}$ is the ambient gas density, and $\rho_{\rm b}$ is the density of the cavity. As the influence of the jet wanes, the cavity will start to rise outward under control of the bouyant force. Its terminal speed, determined by balancing the buoyant force against the drag force, is then $v_{\rm t} \simeq \sqrt{2gV/(SC)} \simeq (4v_{\rm K}/3)\sqrt{2r/R}$, where S is the bubble's cross section, and C is the drag coefficient (Churazov et al. 2001). The second form is for a spherical cavity of radius, r, at a distance R from the cluster center, with $C = 0.75$ (Churazov et al. 2001). The Kepler speed, $v_{\rm K} = \sqrt{gR}$, is comparable to the local sound speed, so that the terminal speed is almost invariably subsonic. In practice, the volume, V, is determined from X-ray measurements of the projected size of a cavity. Because the cavities generally lie within the body of the central galaxy, g can be estimated using the local stellar velocity dispersion, under the approximation that the galaxy is an isothermal sphere, as $g \simeq 2\sigma^2/R$. Alternatively, the gravitating mass distribution can be determined on the assumption that the surrounding gas is hydrostatic, as outlined in Section 1.2, then used to calculate the gravitational acceleration.

Three estimates are commonly used for cavity ages: the buoyant rise time, the refill time, and the sound crossing time. From above, the time taken for a bubble to rise at its buoyant terminal speed from the center of the cluster to its present location, i.e., its buoyant rise time, is approximately $t_{\rm buoy} \simeq R/v_{\rm t} \simeq R\sqrt{SC/(2gV)}$. This is a reasonable estimate for the age of a cavity at late times, long after it has detached from the jet that formed it. The "refill time" is the time required for gas to refill the displaced volume of the cavity as the bubble rises, i.e., the time taken for a cavity to rise buoyantly through its own diameter. If a cavity is formed rapidly and the jet then shuts down, this is an upper limit to the time taken by the cavity to move away from where it formed, hence to its age. In the notation above, $t_{\rm r} = 2\sqrt{r/g}$. As discussed, the early expansion of a cavity is likely to be supersonic, whereas motion of cavities under the control of buoyancy is almost invariably subsonic. Employing the simple compromise assumption, that a bubble is launched from the nucleus and travels at approximately the sound speed, it follows that the time it takes to rise to its projected position is then the sound crossing time, $t_{\rm c} = R/c_{\rm s}$. The sound speed is given by $c_{\rm s} = \sqrt{kT/(\mu m_{\rm H})} \simeq 1100T_5^{1/2}$ km s^{-1}, where the ratio of specific heats, $\gamma \simeq 5/3$, and $\mu \simeq 0.62$. Generally, $t_{\rm c} < t_{\rm buoy} < t_{\rm r}$ for observed cavities.

Which timescale best approximates the true age depends on several unknown factors. Viscous stresses (Reynolds et al. 2005) and magnetic stresses (De Young 2003) can reduce the terminal speed, so that the estimate given here may be high, causing ages to be underestimated and cavity powers to be overestimated. However, equating the age to the buoyant rise time presumes that cavity dynamics are controlled entirely by buoyancy. There are at least a few instances where this is clearly not so.

Other unknown factors include the trajectory with respect to the plane of the sky and the effective location at launch. Projection causes rise times to be underestimated, but generally by less than a factor of two. If cavity dynamics

are controlled by the jet, all of the age estimates above are too long and powers would likewise be underestimated. Although adiabatic cavities expand as they move outward, the ratio r/R is invariably a decreasing function of R, so that the relatively large observed values of r/R (Figure 5) add weight to the argument that most observed cavities have been caught early, before, or soon after becoming buoyancy dominated. Thus, outburst ages may generally be overestimated rather than underestimated.

For example, consider the outburst in Hydra A, for which shock models give a robust age estimate of $\simeq 1.4 \times 10^8$ year (Nulsen et al. 2005b). The buoyant rise time for its large northern cavity (cavity E of Wise et al. 2007) is 5.2×10^8 year, some three to four times longer. This discrepancy would be expected if the dynamics of the cavities in Hydra A are still under the control of the jet. The same applies to most systems with shocks closely surrounding the cavities, and it is likely that shocks will be detected in deeper exposures of many more cavity systems. Because the shocks are relatively weak in most systems, their cavities cannot be advancing much faster than the speed of sound. Thus we get a crude estimate of cavity age from the sound crossing time. We note that this still overestimates the age of the northern cavity of Hydra A by a factor $\simeq 2$.

3.6 Stability of Cavities

A significant issue is cavity disruption, which, in effect, can make cavities nonadiabatic. Buoyant cavities are prone to Rayleigh-Taylor and shear instabilities (e.g., Brüggen & Kaiser 2001; Soker et al. 2002), which can disrupt them, mixing all or part of their contents with the surrounding gas. The fate of a cavity's energy then depends on its constituents. Highly energetic particles can diffuse over large distances without depositing much of their energy as heat (e.g., Böhringer & Morfill 1988). Lower energy particles (such as nonrelativistic protons) will deposit energy locally. The fate of magnetic energy is unclear. Leakage of particles and fields may account for the radio mini-halo and extended nonthermal X-ray emission in the Perseus cluster (Sanders et al. 2005).

Abell 2052 is an example of a cavity system in the throes of disruption. The rim surrounding its northern cavity appears to be breaking apart where radio plasma is leaking out (Blanton et al. 2001). M87 is the nearest cavity system in a cluster and one of the best studied. Its "bud" cavity is strongly suggestive of instability (Forman et al. 2005). However, the numerous small cavities in M87 (Forman et al. 2007) suggest that cavities can fragment without being destroyed. Furthermore, the highly irregular shapes of the cavities in the simulations that demonstrate strong instability are at odds with the apparently regular shapes of observed cavities, also suggesting that real cavities are more stable than the simulated ones.

Magnetic draping (Lyutikov 2006) may help to explain this. A buoyant cavity can entrain magnetic field from the surrounding gas, stretching it and naturally creating a dynamically significant magnetic field around itself. Magnetohydrodynamic simulations suggest that this effect, together with internal cavity fields, can help to stabilize cavities (De Young 2003; Robinson et al. 2004; Jones & de Young 2005). Growth rates of instabilities are also affected by the viscosity (Reynolds et al. 2005; Kaiser et al. 2005), which is poorly known (Section 1.5). As noted by Pizzolato & Soker (2006), while a cavity is being inflated by a jet, its surface is often decelerating. Early in the lifetime of the cavity, the

deceleration can exceed the local acceleration due to gravity, preventing Rayleigh-Taylor instability. As discussed in Section 5.1, cavities that survive rising through several pressure scale heights, whether whole or as fragments, will liberate a significant part of their enthalpy as thermal energy in their wakes.

3.7 Radio Lobe Composition Inferred from X-Ray Observations of Cavities

Extragalactic radio sources are essentially bipolar outflows of magnetic field and relativistic particles ejected from an AGN (Burbidge 1956; Blandford & Rees 1974; Begelman et al. 1984; De Young 2001; Harris & Krawczynski 2006). Their structure includes a core associated with the AGN, oppositely collimated jets emanating from the core, and lobes that bloom from the jet terminals. Jets are narrow, collimated conduits that transmit mass, momentum, energy, and electromagnetic field from the nucleus to the lobes, which in turn transmit much of the energy to the surrounding medium. Radio sources emit synchrotron radiation throughout the radio (and sometimes optical and X-ray) spectrum, from relativistic electrons gyrating along magnetic field lines. Synchrotron radiation reveals only the existence of relativistic electrons and magnetic fields, not their momentum flux and power (Begelman et al. 1984; Harris & Krawczynski 2006). Charge neutralizing particles, such as protons for example, could carry most of the momentum without betraying their existence through the emission of radiation. We will focus on the lower synchrotron power FR I radio sources found in clusters, rather than the higher synchrotron power FR IIs associated with powerful radio galaxies and quasars. Cavities and the associated shock fronts function essentially as gauges of the total energy output of jets, and they allow the contents of radio jets and lobes to be studied with greater certainty than was previously possible. These studies are revealing that even the jets of faint synchrotron sources can carry powers comparable to the luminosities of powerful quasars.

The energy content of radio lobes is at least the sum of energy in particles, $E_{\rm p}$, and magnetic field, E_B;

$$E_{\rm tot} = E_B + E_{\rm p} = \Phi V \frac{B^2}{8\pi} + (1+k) A L_{\rm syn} B^{-3/2}, \tag{6}$$

where V is the lobe volume, and Φ is the volume filling factor of the magnetic field, B. The energy in electrons is related to the radio power per unit frequency, $L_{\rm syn}$, as $E_{\rm e} = A L_{\rm syn} B^{-3/2}$. The unknown factor, k, accounts for unseen particle species (Dunn & Fabian 2004; Govoni & Feretti 2004; De Young 2006), so that the total particle energy can be expressed as $E_{\rm p} = (1+k)E_{\rm e}$. Corresponding approximately to the minimum energy condition (Govoni & Feretti 2004; De Young 2006), it is customary to assume energy equipartition between magnetic field and particles, yielding

$$B_{\rm eq} = \left[\frac{4\pi(1+k) A L_{\rm syn}}{\Phi V} \right]^{2/7}. \tag{7}$$

For electron Lorentz factors of a few thousand, synchrotron radiation at radio frequencies requires $\sim \mu$G magnetic field strengths. If the magnetic field strength greatly exceeds the equipartition value the magnetic field would control the jet dynamics. If the field strength is substantially below the equipartition value, the

particle pressure controls the dynamics. No models of magnetic field-dominated jets have been found to be stable over decades of scale, from the Schwarschild radius to the lobes, and thus it seems unlikely that the energy density in magnetic fields greatly exceeds that of particles (De Young 2006).

The internal energy of the cavity, $E_{\rm tot}$, as well as its filling factor, Φ, and magnetic field strength, B, can be constrained by X-ray observations. As discussed in Section 5.1, the internal energy ranges from pV for a magnetically dominated cavity to $3pV$ for a lobe dominated by relativistic particles (this is the enthalpy minus the work of inflation, pV). The gas pressure surrounding a cavity provides a measure of the energy density in field and particles required to support it against collapse. Several studies have shown that at equipartition, lobe pressures are approximately an order of magnitude smaller than the surrounding gas pressure (Blanton et al. 2001; Fabian et al. 2002; De Young 2006). One way around this is to suppose that the filling factor of the radio plasma, Φ, is less than unity. In that case, if the radio plasma is in equipartition at the external gas pressure, p, its filling factor would be $\Phi = (p_{\rm eq}/p)^{7/4}$, where $p_{\rm eq}$ is the equipartition pressure determined assuming a filling factor of unity. Thus, the filling factor of the radio plasma might be only percents and total lobe energies reduced by similar factors.

However, this possibility has been ruled out by X-ray observations of cavities and shocks. X-ray count deficits over lobes are typically consistent with the X-ray emitting gas being completely excluded from radio lobes. While it is difficult to place stringent limits on the amout of X-ray emitting gas within lobes, cavities would not be evident in X-ray images unless the lobes displace most of the X-ray emitting gas. Furthermore, the expanding radio lobes are the pistons that drive shocks into the surrounding gas. To obtain significant shocks, the work done by an expanding lobe, $\int p\,dV$, must be comparable to $p_{\rm s}V_{\rm s}$, where $p_{\rm s}$ is the preshock pressure and $V_{\rm s}$ is the volume encompassed by the shock. For known shocks, this generally requires the lobes to displace most of the gas within the volume they occupy, i.e., it demands filling factors, Φ, close to unity. The pressure support could then be supplied by some combination of thermal or relativistic particles.

De Young (2006) modeled radio jets as pipe-like conduits of energy collimated by the surrounding gas pressure. The energy flux was inferred from the pV work and buoyancy ages, based on X-ray observations alone, while the lengths and cross sections of the jets were taken from high-resolution radio observations. De Young (2006) found that the energy in pV work alone is so large that the jets would decollimate unless most of the energy and momentum are carried by cold, heavy particles (e.g., protons) that do not contribute significantly to the internal isotropic pressure of the jet (but see Dunn, Fabian & Celotti (2006) for a discussion of electron-positron jets). De Young's results are consistent with the high ratio of relativistic particle energy to electron energy (k) found by Dunn, Fabian, & Taylor (2005). Despite the many unknowns concerning, for example, jet stability, confinement, and acceleration mechanisms, De Young's analysis suggests that electrons are unable to supply the observed jet power alone and must be aided by heavy particles, or perhaps Poynting flux.

The fluid supporting the cavities could be dominated by a hot thermal plasma, or cosmic ray pressure (Mathews & Brighenti 2007). Constraints on such a fluid can be placed by asking what combination of gas temperature and density would be required to provide pressure support without violating the X-ray surface brightness constraints. This technically challenging measurement has yielded constraints for a few systems of $kT \gtrsim 15$ – 20 keV (Nulsen et al. 2002;

Blanton et al. 2003).

Sunyaev-Zeldovich (SZ) measurements in the submillimeter band in principle provide a novel means to discriminate between a thermal and nonthermal cavity fluid (Pfrommer et al. 2005). The SZ decrement is sensitive only to thermal gas. Thus the presence or absence of a decrement toward the cavities themselves would provide a test. The effect is subtle and the observations are difficult to perform using existing instrumentation, but should be possible in the future with the Atacama Large Millimeter Array (ALMA; Pfrommer et al. 2005). These measurements coupled to deeper X-ray observations have the potential to place valuable new constraints on the composition of radio jets. In the longer term, SZ effect can also be used to detect shock fronts (Cavaliere & Lapi 2006). Likewise, GLAST may place interesting constraints on the cosmic ray content of cavities through observations of the pion decay continuum produced in cavity walls (Mathews & Brighenti 2007).

3.8 Radiative Efficiency of Radio Sources

The plot of jet power determined from X-ray cavity data versus total synchrotron power (core plus lobes) in Figure 7 shows a trend, as one might expect. The median ratio of jet (cavity) power to synchrotron power is ~ 100 (Bîrzan et al. 2004). However, the mean is much larger ~ 2800 owing to the large scatter. When considering radio flux from the lobes alone, the average ratio rises dramatically to ~ 4700 (L. Birzan, private communication). Figure 7 clearly demonstrates that most of the jet power is deposited into the surrounding medium and that a negligible fraction is radiated away. Although this result is not terribly surprising in a qualitative sense, we now have a quantitative measurement of this ratio that, interestingly, is on the high side of theoretical expectations (e.g., De Young 2001). Furthermore, the large scatter in the relationship, ranging between unity and several thousand, shows that synchrotron luminosity is a poor measure of true jet power. Factors contributing to the scatter include variations in age, field strength, and jet composition, but how these variables combine to create the scatter is not understood. Several radio faint cD galaxies with jet powers that equal or exceed the energy output of powerful quasars and radio sources like Cygnus A have been identified through X-ray observations, yet they would not have been identified as such using optical and radio observations alone. X-ray observations have revealed that under some circumstances black holes produce powerful mechanical outflows with little accompanying radiation.

It is worth noting that adopting a pV-based standard for AGN energy output blurs the canonical separation between high-power FR II radio sources and lower-power FR I radio sources that are typically found in the centers of clusters. Cygnus A is the best known FR II radio source, and is the most powerful radio source in the 3C catalog within z = 1 (cf. Young et al. 2002). Seven objects in the Rafferty et al. (2006) sample of cavity systems exceed Cygnus A in mechanical power, yet none of them are considered to be powerful radio sources. The most distant object in the sample lies at $z \sim 0.5$, but most lie within $z \sim 0.2$.

3.9 Simulations of Mixing by Radio Lobes

The rising abundance gradients found in the cores of cD clusters are presumably established over a few gigayears by stellar evolution in cD galaxies. The gradients

should in principle then be sensitive to erasure by mixing induced by merger and AGN activity over that time frame, thus providing interesting constraints on both the outburst and merger history, as well as jet entrainment models.

AGN-induced mixing has been explored recently by several groups using 2D and 3D hydrodynamical simulations (Brüggen 2002; Omma et al. 2004; Heath et al. 2006; Roediger et al. 2006). The studies generally assumed an initial metallicity gradient added to a β-like model atmosphere with gas particles tagged by metallicity. Moderate jet powers of 1.4×10^{41} erg s^{-1} to 6×10^{43} erg s^{-1}, and quasar-like jets exceeding 10^{46} erg s^{-1} lasting 100 Myr to 3 Gyr have been explored. Roediger et al. (2006) tailored their simulation to the conditions in Perseus and included a prescription for metal injection from the central galaxy.

These studies found that lower power jets allowed to run for 100 Myr or so produced only modest dredging that reduced existing metallicity gradients by at most a few tens of percent. However, Heath et al. (2006) found that quasar-like outbursts are able to reduce metallicity gradients to roughly 10% of their initial values by transporting the metals outward, primarily through convection and entrainment behind the cavities. Short duration (powerful) jets producing big cavities, and wide jets were most effective. Simulations generally produce anisotropic abundance distributions aligned along the jet axis, a prediction that can be tested using available X-ray and radio observations. However, these studies considered jets launched at constant aspect angles into static atmospheres. An isotropic distribution of metals could be preserved through turbulent mixing and gas circulation (e.g., Mathews & Brighenti 2003; Heinz et al. 2006) or by launching bubbles on random trajectories, perhaps through jet precession, as has been observed in some clusters (e.g., Gitti et al. 2006).

3.10 Observations of Outflows and Mixing

The outward mixing of metal-enriched gas has been invoked to explain why central metallicity peaks are broader than the light profiles of cD galaxies (e.g., David et al. 2001; De Grandi & Molendi 2001; Rebusco et al. 2005). Moreover, there are several striking examples of plumes and shells of metal-enriched plasma and cold clouds that were apparently dragged outward by radio jets and lobes advancing into the ICM. A metal-enriched shell of gas was found nearly 90 kpc from the nucleus of NGC 1275 in the Perseus cluster (Sanders et al. 2004), and a plume of cool, X-ray emitting gas extends several tens of kpc along the radio axis of Hydra A (Nulsen et al. 2002). A metal-rich shell or cap of gas was found near the edge of the southern cavitiy, 34 kpc from the nucleus of the central galaxy in the HCG 62 group (Gu et al. 2007). However, the absence of a similar feature associated with the northern cavity and other circumstantial evidence for merger activity lead the researchers to propose the gas may have been stripped from an interloping galaxy. Arcs and shells of Hα emission surround the cavities and radio sources in several clusters (Blanton et al. 2001; Fabian et al. 2003b; Crawford et al. 2005; Hatch et al. 2006), and cold molecular gas surrounds the inner cavities in the Perseus cluster (Salomé et al. 2006). The cooling time of the hot gas near the cavities is too long for the gas to have cooled locally, so it was probably dragged there from below.

4 STABILIZING COOLING FLOWS BY FEEDBACK

4.1 Heating and Cooling Rates in Clusters

The failure to find large quantities of cooling gas with the expected properties of a cooling flow (Peterson et al. 2003) implies that more than 90% of the energy radiated away is being replenished. Only a few percent of the gas associated with the cooling flow forms stars and even less accretes onto the central supermassive black hole. For an AGN to be a viable agent, it must be powerful, persistent, an efficient heater, and it must distribute the heat throughout the cooling region. If jets are underpowered, the remaining issues are moot.

As discussed in Section 2, in terms of the classical cooling flow model, the power radiated from the core of a cluster can be expressed as $L_{\rm X} \simeq 1.3 \times 10^{44} T_5 \dot{M}_2$ erg s^{-1}, where the classical cooling is given by $\dot{M}_2 = \dot{M}/(100\ {\rm M}_\odot\ {\rm year}^{-1})$. This radiated power is equivalent to $\sim 10\%$ of the gravitational binding energy released by only $\simeq 0.02\ {\rm M}_\odot\ {\rm year}^{-1}$ of accretion onto a black hole. The fact that AGN outbursts are so frequently associated with cool and cooling X-ray atmospheres suggests that the rates of cooling and AGN heating may be thermostatically controlled. Three lines of evidence draw us to this conclusion. First, central cooling times are as short as $\sim 3 \times 10^8$ year, $\sim 1/30$ of the Hubble time, in many clusters and they are even shorter in elliptical galaxies (Voigt & Fabian 2004). The $\sim 100\ {\rm M}_\odot\ {\rm year}^{-1}$ of cooling gas expected in the classical cooling flow model is rarely observed, implying that the energy radiated is being replenished on a shorter timescale than the small cooling times found within ~ 10 kpc of the nucleus (Nulsen et al. 2005b).

If the heating rate were not tied to the radiative cooling rate, then it must exceed it to ensure that very little gas cools to low temperatures in the majority of cooling flows. This would only be possible if the heating rate exceeded typical cooling rates, giving rise to net heating of the ICM. Net heating would then drive up the central entropy, and in the long-term, the central cooling times would approach the ages $\sim H_0^{-1}$ of most clusters, in contradiction of observations. Thus, it is difficult to maintain a significant proportion of clusters, groups, and galaxies with short central cooling times, unless heating rates are tied to cooling rates by some feedback loop. Second, the trend between cavity-based power estimates and the X-ray luminosity of cooling gas shown in Figure 8, strongly implicates AGN: they apparently know about the cooling gas and vice versa. Third, the entropy profiles of the gas in cooling flows fall inward in roughly power-law fashion (Piffaretti et al. 2005), but often flatten in the cores (Donahue et al. 2006) implying entropy (energy) input at a level of ~ 10 keV cm^2 (McCarthy et al. 2004; Voit & Donahue 2005), which is consistent with the observed level of AGN energy input. The flattening is seen in both radio active and radio quiet clusters. It suggests the operation of an intermittent heating mechanism that maintains a roughly steady power when averaged over times comparable to the central cooling time. The coincident rates (70%) of cavities (Dunn et al. 2005) and radio emission (Burns 1990) in cooling flow clusters further implicates AGN, although heat conduction or other agents may augment AGN heating (Ruszkowski & Begelman 2002; Brighenti & Mathews 2003).

A quantitative comparison between X-ray (cooling) luminosity and jet power (heating) averaged over the lifetime of a cavity $pV/t_{\rm bub}$ is shown in the heating versus cooling diagram (Figure 8) taken from Rafferty et al. (2006). In this dia-

gram, the cooling luminosity is the radiated power that must be replenished by heating. This quantity is found by subtracting from the total X-ray luminosity within the cooling radius the luminosity from gas that could be condensing out without violating observations. This correction amounts to less than 10% of the total X-ray luminosity. The diagonal lines in Figure 8 represent equality between heating and cooling assuming pV, $4pV$, and $16pV$ of heat input per cavity. Cavities filled with a nonrelativistic monoatomic gas ("hot bubbles") would supply approximately $2.5pV$ per cavity, whereas cavities filled with relativistic gas would supply roughly $4pV$ per cavity (Section 5.1). The true effective energy per cavity could be substantially greater than $4pV$ if much of the outburst energy has been dissipated by shocks (Section 5.4), or if other cavity systems exist below the threshold of detectability. Thus, the data points should be treated as lower limits.

More than half of systems with detectable cavities liberate enough energy to balance or exceed radiation losses at the present time. Other systems including those without detectable cavities do not. Either this implies that AGN require help from other energy sources in order to suppress cooling, or it reflects the elusive nature of X-ray cavities and the transience and variable power output of AGN. If AGN outbursts are transient, then the time averaged AGN heating power needs to match the power radiated. Additional energy supplied by AGN associated with the broader cluster galaxy population (Nusser et al. 2006) will heat the gas beyond the cooling region but is apparently inconsequential within the cooling region itself (e.g., Best et al. 2007).

The trend in Figure 8 does not take account of the 30% of cooling flow clusters that lack identifiable cavities (Dunn & Fabian 2006), which would in principle populate the lower right-hand side of the diagram. It is not known whether such objects have had AGN activity in the recent past, but the associated cavities and shock fronts are not visible in existing data, or whether other heating mechanisms are at work. Given that deeper observations have invariably revealed more structure (e.g., Forman et al. 2007), there is good reason to suspect that the fraction of clusters for which the AGN power is sufficient to balance radiative losses will grow beyond half as deeper Chandra images become available.

Regardless of this, the existing data already suggest that AGN heating can balance cooling. For the sample of Rafferty et al. (2006), the mean cooling power is 6.45×10^{44} erg s^{-1}, while the mean cavity power is 1.01×10^{45} erg s^{-1} (using $4pV$ per cavity and the bouyant lifetimes). Assuming that cooling flow clusters without evident cavities have similar cooling powers and zero cavity power, we can correct the ratio of mean cavity power to cooling power for these with a factor of 0.7 (Dunn & Fabian 2006), giving 1.1 for this ratio. Thus, within the substantial uncertainties, it is plausible that time averaged AGN heating powers balance radiative cooling. A more accurate assessment of the ratio of heating to cooling must await a study of a complete, unbiased sample of cooling flow clusters.

If we assume for the moment that all cooling flows are suppressed by AGN, the scatter in Figure 8 may be a consequence of variable AGN power output. Nipoti & Binney (2005) modeled AGN power output as a Gaussian process with a log-normal distribution at a fixed cooling luminosity, and an observationally motivated outburst timescale of 10^8 years. Their model implies that in any given system there is a good chance of finding smaller than average jet powers, because much of the power is generated by less frequent but more powerful outbursts. In

this context, the objects falling below the $2pV - 4pV$ lines may be in a lower than average outburst state and thus may be in or moving toward a cooling cycle. In the Nipoti & Binney (2005) model, the powerful, rare outbursts are experienced by all systems. These outbursts may be responsible for the high entropy pedestals observed in radio quiet cD galaxies (Donahue et al. 2006; Pope et al. 2006).

How effective AGN heating is over the lives of clusters depends on how and how much their power output varies over time. Although AGN power output is a strong function of halo gas mass, power outputs vary widely at a given mass. The systems with the largest cavities represent the extreme in power output. We do not know whether they are unique to some clusters or whether all systems occasionally experience them. These rare but powerful outbursts can easily dominate a cD galaxy's AGN power output over the age of a cluster.

To summarize, under the assumptions outlined above, AGN are powerful enough to supress cooling in many and perhaps all cooling flow systems. However, this conclusion depends on how well the X-ray method traces true jet power and how efficiently cavity enthalpy and shock energy is converted to heat.

4.2 Heating and Cooling in Elliptical Galaxies and Groups

The cooling time of the hot gas in the centers of some gE galaxies is less than $\sim 10^8$ year, which is shorter than found in the cores of clusters. As in clusters, the hot gas there is expected to cool and form stars in the host gEs, yet it fails to do so at the expected rates of ~ 1 $M_\odot$ year^{-1} (Mathews & Brighenti 2003). Like clusters, many gEs have cavities or other disturbances in the hot gas implicating AGN as significant heating agents (Mathews & Brighenti 2003; Diehl & Statler 2007). Jones et al. (2007) have assembled Chandra X-ray observations of a nearly complete sample of roughly 160 nearby gE galaxies, 109 of which show significant diffuse emission from hot gas. Of those, 27 have significant AGN cavities. Nulsen et al. (2007) evaluated the relative rates of AGN heating and radiative cooling for the 27 ellipticals with detectable cavities, giving the results shown in Figure 9. Apart from minor differences, this figure can be viewed as extending Figure 8 to less massive halos. Although heating matches or exceeds cooling in roughly half of the cluster systems in Figure 8, AGN power exceeds radiative losses in all but one or two of the nearby gEs shown in Figure 9. Roughly one quarter of Jones's gEs with significant emission from hot gas have detectable cavities, a detection rate that is similar to the overall rate of detection in clusters, but is smaller than the 70% detection rate in cluster cooling flows (Dunn et al. 2005). Based on central cooling times, all 109 of the gEs with significant hot atmospheres are cooling flows. Assuming $1pV$ per cavity, the total heating power of the 27 nearby gEs harboring cavity systems is $\sim 2 \times 10^{43}$ erg s^{-1}. This is to be compared to the total cooling power of $\sim 10^{44}$ erg s^{-1} for all 109 nearby gEs with significant emission from hot gas. Allowing for a cavity enthalpy of $4pV$ for relativistic gas and the significant boost to this owing to shock energy, overall heating and cooling powers for the nearby gE sample match reasonably well. Although there is still significant systematic uncertainty, it seems that intermittent AGN outbursts are a plausible mechanism for preventing X-ray emitting gas from cooling and forming stars in nearby gE galaxies. A similar result was found indirectly for gEs culled from the Sloan survey by Best et al. (2006), who determine jet power by assuming a one to one correspondence with radio power, calibrated using cavity data from Bîrzan et al. (2004).

Because the binding energy per particle is lower in groups, the same nongravitational heating energy per particle will have a greater effect in groups than in clusters. Rosat studies of poor clusters and groups reported an "entropy floor" or pedestal in the gas entropy profile (e.g., Ponman et al. 1999). It was argued that the entropy floor caused the steepening in the luminosity versus temperature relation, which was more pronounced at group masses. Entropy floors can be produced by a number of processes, including AGN outflows, supernova driven galactic winds, and by the effects of cooling (Voit 2005). With higher resolution data from Chandra the situation has become murkier. Entropy floors are no longer seen, but there is an apparent excess of entropy at larger radii, beyond the inner cooling region (Ponman et al. 2003). Mushotzky (2004) has argued that the steeper than self similar power law scaling of luminosity versus temperature for rich clusters extends to groups, but with a larger scatter at the group scale.

Unfortunately, AGN heating is not as well studied in groups as in clusters. We know that the gas in many groups is being disturbed by radio sources emanating from their central galaxies (Croston et al. 2005), for example, as seen in HCG 62 (Morita et al. 2006; Nakazawa et al. 2007). The cavity power of the lobes is sufficient to quench the cooling flow but the overall significance of AGN heating in groups is unclear (Dwarakanath & Nath 2006).

The effects of AGN heating on intragroup gas has been explored by separating X-ray bright systems with central galaxies into radio-loud and radio-quiet bins. Analyzing an X-ray-selected sample of groups, Croston et al. (2005) found that in 63% of groups with a dominant central elliptical galaxy the dominant elliptical harbors an active radio source. Many of these radio sources are interacting with the hot gas filling the groups. Croston et al. (2005) found that the radio loud groups are slightly hotter on average at a given X-ray luminosity than radio quiet groups, which they attribute to AGN heating. They point out that AGN heating at the level they find extending over 5×10^9 year would be able to supply the ~ 1 keV per particle of excess energy required to preheat groups (e.g. Voit & Donahue 2005).

However, in a Chandra study of 15 groups, Jetha et al. (2007) found only modest steepening of the gas temperature in radio-loud groups compared to radio-quiet ones, and steeper entropy gradients in groups with brighter central galaxies and presumably more massive nuclear black holes. It is unclear whether these trends implicate AGN heating or heating by the galaxies themselves. Jetha et al. found power law entropy profiles extending to small radii, and only small differences in the gas profiles of radio-loud and radio-quiet groups. They found that AGN heating may have a more significant effect in quenching cooling than for preheating.

4.3 Uncertainties in Estimating Jet Power

Model assumptions about the time and energy dependence of outbursts are a significant source of uncertainty in the calculation of mean cavity (jet) power. If AGN inject energy in a series of short, isolated outbursts, the interval between outbursts characterizes $t_{\rm bub}$. This interval is impossible to estimate for individual systems in the absence of multiple generations of cavities, such as those in Perseus (Fabian et al. 2000) and Abell 2597. Multiple cavity systems are also required to estimate the mean energy per outburst. The ghost cavities in Perseus and Abell 2597 imply an outburst every 60 - 100 Myr or so, and in both clusters

the earlier outbursts were stronger than the current ones, indicating variability in outburst strength. The ripples in Perseus indicate that some outbursts may occur on shorter timescales than the cavity ages, implying the outburst period is also variable.

If outbursts are more nearly continuous, i.e., the jets remain active for a substantial fraction of the outburst cycle, then the current jet power is a more useful measure of the average value. In general, the off-time must be included to measure a population average. The large systems (Hydra A, MS0735.6+7421, Hercules A) appear to be operating in this mode (e.g., Wise et al. 2007). Most observational treatments implicitly assume a more nearly continuous distribution of outbursts.

Sources of uncertainty in the measurements of cavity energy include the volume estimates from the projected cavity sizes and shapes and the unknown composition of the cavity plasma, which combined give an uncertainty of at least a factor of several. In addition, the energy per outburst is probably underestimated owing to adiabatic losses, cavity disruption, undetected cavities, and the omission of shock energy (e.g., Nusser et al. 2006; Binney et al. 2007). These effects are offset to some degree by the unknown fraction of outburst energy that is converted to heat.

5 HEATING MECHANISMS

5.1 Cavity Heating

The energy required to create X-ray cavities around radio lobes is the sum of the pV work required to displace the X-ray emitting gas and the thermal energy of the contents of the lobe, i.e., the enthalpy,

$$H = E + pV = \frac{\Gamma}{\Gamma - 1} pV,$$

where p is the pressure in the lobe and V is its volume. The second form applies if the lobe is filled with an ideal gas with constant ratio of specific heats, Γ. If the lobe is dominated by relativistic particles, $\Gamma = 4/3$ and $H = 4pV$, whereas if it is dominated by nonrelativistic gas, $\Gamma = 5/3$ and $H = 2.5pV$. Lobes may also be dominated by magnetic field, in which case $H = 2pV$. Other possibilities lie between these extremes, so that, although the equation of state (Γ) for lobes is not known, lobe enthalpy is likely to fall in the range $2pV$ - $4pV$.

Simulations show that buoyant cavities can heat the surrounding gas as they rise through a cluster atmosphere (Brüggen & Kaiser 2002; Reynolds et al. 2002). Churazov et al. (2002) argued that essentially all of the enthalpy of a rising cavity can be thermalized in its wake and a simple mechanism for this is outlined in (Bîrzan et al. 2004). As a buoyant cavity rises, some X-ray emitting gas must move inward to fill the space it vacates (Figure 10), so that gravitational potential energy is turned into kinetic energy in the ICM. The potential energy released as a cavity rises a distance δR is

$$\delta U = Mg\,\delta R = V\rho g\,\delta R = -V\frac{dp}{dR}\,\delta R = -V\,\delta p, \qquad (8)$$

where $M = \rho V$ is the mass of gas displaced by the cavity, V is its volume, ρ is the density of the surrounding gas and g is the acceleration due to gravity. The third equality relies on the surrounding gas being close to hydrostatic equilibrium,

so that $\rho g = -dp/dR$. The last equality expresses the result in terms of the change in pressure of the surrounding gas over the distance δR, $(dp/dR)\,\delta R = \delta p$. Because the rising cavity moves subsonically (Churazov et al. 2001), its pressure remains close to that of its surroundings and we may regard this as the change in its pressure. The first law of thermodynamics, $dE = TdS - pdV$, expressed in terms of the enthalpy is $dH = TdS + Vdp$. Entropy remains constant for an adiabatic cavity (radiative losses from the cavity are negligible), so that this gives $\delta H = V\,\delta p$. Thus, Equation 8 shows that the kinetic energy created in the wake of the rising cavity is equal to the enthalpy lost by the cavity as it rises.

Regardless of the viscosity, we should expect this kinetic energy to be dissipated, creating heat locally in the wake of the cavity. If the viscosity is high, i.e., the Reynolds number is low, the motion is damped viscously in a laminar wake that is comparable in size to the cavity. If the Reynolds number is high, the wake is turbulent and kinetic energy is damped on the turn-over timescale of the largest eddies (also comparable to the size of the cavity). The turbulent cascade maintains the dissipation rate by propagating energy to sufficiently small scales for viscous dissipation to keep pace (in fact, the turbulent spectrum is fully characterized by the dissipation rate; Landau & Lifshitz 1987). In both cases, kinetic energy is damped before diffusing far from the axis on which the cavity rises. This leads to the important result that the enthalpy lost by a buoyantly rising cavity is thermalized locally in its wake, almost regardless of the physical properties of the cavity and the surrounding gas.

Heating by cavity enthalpy is the physical basis of the "effervescent" heating model (Begelman 2001; Ruszkowski & Begelman 2002; Roychowdhury et al. 2004). Chandra observations have established not only that cavities are common, but also that many clusters contain multiple cavities, though not all coincident with active radio lobes (Fabian et al. 2000). The numerous cavities seen in deep observations of M87 (Forman et al. 2007) also fit this model. The enthalpy of an adiabatic cavity depends on the surrounding pressure as $H_{\rm b} = H_{\rm b,0}(p/p_0)^{(\Gamma-1)/\Gamma}$, where $H_{\rm b,0}$ is the initial enthalpy of the cavity and p_0 is its initial pressure. If the mean power injected by an AGN as cavity enthalpy is $L_{\rm b}$, then the mean heating rate per unit volume averaged over the sphere at radius R due to liberated cavity enthalpy is

$$\Pi_{\rm b} = -\frac{L_{\rm b}}{4\pi R^2}\frac{d}{dR}\left(\frac{p}{p_0}\right)^{(\Gamma-1)/\Gamma}, \tag{9}$$

where p_0 is the pressure at the radius, R_0, where the cavity is formed. The value of R_0 depends on outburst details, but it is always nonzero. Very little cavity enthalpy is thermalized within R_0. With minor modifications, this is the effervescent heating rate used by Begelman (2001) and successors. Using this model, Ruszkowski & Begelman (2002) argued that cavity enthalpy needs to be supplemented by thermal conduction from the surrounding cluster in order to prevent cooling. However, Roychowdhury et al. (2004) find that this conclusion depends on the assumed total rate of AGN heating. Note that these are all 1D models, employing mixing length theory to model convection. Such models probably omit significant features of the full, 3D flow.

As well as providing better models for the convection associated with anisotropic cavity heating, 3D simulations allow more realistic treatments of cavity stability and mixing (Quilis et al. 2001). Dalla Vecchia et al. (2004) made 3D hydrodynamic simulations for the longer-term effects of cavity heating by injecting energy

to simulate the formation of radio lobes at random positions with a Gaussian distribution around cluster centers. Although they found that the resulting heat input can prevent catastrophic cooling, their model clusters do not produce cool cores as observed. They argue that additional preheating, taking place earlier in the collapse hierarchy, could resolve this disagreement. AGN heating rates in this model are fixed, not determined by feedback, and Dalla Vecchia et al. (2004) conclude that prevention of catastrophic cooling is not sensitive to AGN power. A significant channel of heating for their model is the mixing of gas from the simulated cavities with the general ICM. Relativistic particles can be slow to transfer energy to gas (e.g., Böhringer & Morfill 1988) and the fate of magnetic fields is poorly understood, making it unclear how effectively radio plasma mixes with and heats the ICM in practice.

5.2 Heating by Weak Shocks

Although a substantial energy, comparable to the cavity enthalpy, is required to drive the weak shocks seen in association with AGN outbursts in some clusters (Forman et al. 2005; McNamara et al. 2005), much of the shock energy ends up as additional potential energy in the gas. This helps to delay cooling by reducing gas density and increasing the total energy that must be dissipated. However, the key requirement on the process that prevents the gas from cooling is to make up for entropy lost by radiation from the gas. Shock heating probably plays a significant role in this, especially close to the AGN (Fabian et al. 2005). A fundamental distinction between sound waves and shocks is the entropy created by dissipation at shock fronts. For weak shocks, the entropy jump per unit mass, ΔS, is proportional to the cube of the shock strength (e.g., Landau & Lifshitz 1987; David et al. 2001; measured here by the fractional pressure increase, $\delta p/p$, where p is the preshock pressure and δp is the pressure increase across the shock). The equivalent heat input per unit mass is $T\,\Delta S$, where T is the gas temperature. To lowest nonzero order, this equivalent heat input amounts to a mean heating rate per unit volume due to repeated weak shocks of

$$\Pi_{\rm s} = \frac{(\gamma+1)}{12\gamma^2}\frac{\omega p}{2\pi}\left(\frac{\delta p}{p}\right)^3, \qquad (10)$$

where γ is the ratio of specific heats for the ICM and the interval between outbursts is expressed as $2\pi/\omega$ (compare the sound heating rate, Equation 11).

The repeated weak shocks around M87 seen by Forman and colleagues (Forman et al. 2007) demonstrate the possible significance of weak shock heating. Based on its X-ray surface brightness profile, the innermost shock, 0.8 arcmin (4 kpc) from the AGN, has a Mach number of 1.4, so that its equivalent heat input is only 2% of the gas thermal energy. However, there is another comparable shock at about twice the radius, suggesting repeated outbursts every $\sim 2.5\times10^6$ year, while the cooling time of the gas is $\sim 2.5\times10^8$ year. Over the cooling time, this leaves ample time for multiple weak shocks to make up for the energy radiated by the gas (Nulsen et al. 2007). In M87, weak shocks are capable of preventing gas near the AGN from cooling.

When a shock overruns a cavity, the high sound speed of the cavity causes the shock to propagate faster through the cavity than around it. This results in the formation of a vortex ring around the cavity after it has been overrun (Churazov et al. 2001; Enßlin & Brüggen 2002). Heinz & Churazov (2005) note

that this process, an example of Richtmyer-Meshkov instability, can increase the fraction of shock energy that is thermalized in the ICM, especially for weak shocks, because it converts shock energy into localized kinetic energy that can then be dissipated as heat. If the ICM contains many small cavities, Heinz & Churazov find that the attenuation length due to the Richtmyer-Meshkov instability is inversely proportional to the fraction of the ICM occupied by the cavities. For example, if cavities in the Perseus cluster have a filling factor of $\sim 10\%$, most of the energy of the weak shocks would be dissipated within the central 100 kpc. The significance of this process is hard to assess, because small bubbles are not generally accessible to observation. If, for example, bubbles occupy $\sim 10\%$ of the volume of the ICM, then they also contain $\sim 10\%$ of its thermal energy. Because the bubbles rise at their terminal speeds, $v_{\rm t} \simeq v_{\rm K}\sqrt{r/R}$ (Churazov et al. 2001), they must be replaced continually. The power required to maintain a large bubble filling factor is substantial, unless the bubbles are very small, and a large part of that power would be dissipated as bubble heating (Section 5.1).

5.3 Heating by Sound Damping

Repeated weak shocks may also be regarded as a superposition of sound waves. Fabian et al. (2003a) showed that viscous damping of sound waves generated by repeated AGN outbursts may represent a significant source of heating. The heating power per unit volume due to dissipation of a sound wave can be expressed as (Landau & Lifshitz 1987; Fabian et al. 2005)

$$\Pi_{\rm d} = \left[\frac{2\nu}{3} + \frac{(\gamma-1)^2\kappa T}{2\gamma p}\right]\frac{\omega^2\rho}{\gamma^2}\left(\frac{\delta p}{p}\right)^2, \qquad (11)$$

where ρ, T, p and γ are the density, temperature, pressure, and ratio of specific heats of the gas, respectively, κ is the thermal conductivity, ν is the kinematic viscosity ($\nu = \mu/\rho$, where μ is the viscosity), ω is the angular frequency, and δp is the pressure amplitude of the sound wave. This expression includes both viscous and conductive dissipation. Both terms in the leading coefficient have the form of a mean free path times a thermal speed (Spitzer 1962). For an unmagnetized plasma, the mean free paths of the electrons and protons are the same. For the kinematic viscosity, the thermal speed is that of the protons, whereas in the conductive term it is that of electrons. Thus conductive dissipation would be greater in the absence of a magnetic field.

Heating by weak shocks is a separate mechanism from heating by sound dissipation. In numerical simulations, shocks are controlled by viscous stresses (Ruszkowski et al. 2004a,b; Brüggen et al. 2005), so that these two processes are lumped together. Dissipation of sound depends on the transport coefficients, but shock heating does not. Therefore, uncertainty in the transport coefficients (Section 1.5) translates directly into uncertainty in the heating rate due to sound dissipation. If the transport coefficients are suppressed by no more than an order of magnitude, about the range suggested by observations, analytical estimates (Fabian et al. 2003a) and simulations (Ruszkowski et al. 2004a,b; Brüggen et al. 2005) agree that sound dissipation plays a significant role in converting AGN energy into heat in the ICM. The two mechanisms have distinct dependencies on the parameters (Equations 10 and 11), leading to distinct spatial distributions of heating.

Only the fundamental frequency should be used in applying the sound dissipation rate (Equation 11). The thickness of a weak shock front can be expressed as $w \simeq \lambda/(M-1)$, where λ is the effective particle mean free path and M is the shock Mach number (e.g., Landau & Lifshitz 1987). When the width of the shock front becomes comparable to or larger than the wavelength, the disturbance transitions from a shock wave to a sound wave. At this transition the sound dissipation rate, which depends on transport coefficients, and the shock dissipation rate, which does not, cross over. When the thickness of a shock is considerably smaller than the distance between successive shocks, the shock front contributes substantial power in high harmonics when decomposed into a Fourier series. The fundamental frequency is determined by the shock repetition rate. Because the dissipation rate varies as ω^2 (Equation 11) the linear treatment suggests that the high frequency components will dissipate quickly, producing significant heating. However, the entropy created at the shock front is determined entirely by the Rankine-Hugoniot jump conditions, regardless of the transport coefficients. Nonlinear effects adjust shock thickness to make the dissipation rate match that required by the jump conditions. Although shock thickness is determined by the transport coefficients, the dissipation rate for the high frequency terms is not. This dissipation is accounted for as the shock heating rate (Equation 10). Only the dissipation rate of the component at the fundamental frequency depends directly on the transport coefficients and only it should be regarded as subject to sound damping.

In the absence of magnetic fields, the kinematic viscosity, ν, and the coefficient of the conductive dissipation rate, $\kappa T/p$ in Equation 11 both scale approximately with temperature as $T^{5/2}$. If this scaling applies in reality, the sound dissipation rate is sensitive to the ICM temperature, which would reduce its significance in cool systems. However, because the sound dissipation rate is also sensitive to frequency, higher outburst rates in cool systems could offset the reduction in transport coefficients. Fabian et al. (2003a) find that outbursts occur every $\sim 10^7$ year in the Perseus cluster, where the ICM temperature is ~ 4 keV, whereas the period of outbursts in M87 is $\sim 2.5 \times 10^6$ year for an ICM temperature $1-2$ keV (Nulsen et al. 2007). This hints that the feedback process may be able to adjust the frequency as well as the power of AGN outbursts.

5.4 Cavity Enthalpy versus Shock Energy

The division of jet energy between cavity enthalpy and shocks is affected significantly by the history of an outburst. Here, shock energy is used loosely to mean the total work done on the ICM by an inflating cavity, most of which ends up as thermal and gravitational potential energy in the hot gas. In fact, because cavity expansion lifts gas outward, it invariably reduces the gas pressure after a shock has passed. As a result, the gas expands and its total thermal energy is generally decreased after the outburst, especially when shocks are weak. Thus, the ultimate repository for most of the shock energy is probably potential energy in the ICM.

At one extreme, consider a jet that dumps its energy explosively into the gas in a single brief event. Initially this would create a tiny cavity with volume, $V_{\rm i}$, and pressure, $p_{\rm i}$, much greater than the pressure of the surrounding gas. The thermal energy of the cavity, $E_{\rm i} = p_{\rm i}V_{\rm i}/(\Gamma-1)$, would equal the energy deposited by the jet (radiative losses are assumed negligible throughout this process). This cavity

would expand explosively, driving a strong shock into the ICM, until its pressure reached that of its surroundings, $p_{\rm f} \ll p_{\rm i}$. Because the expansion is adiabatic, the final energy of the cavity is

$$E_{\rm f} = \frac{1}{\Gamma - 1} p_{\rm f} V_{\rm f} = \frac{1}{\Gamma - 1} p_{\rm f} V_{\rm i} \left(\frac{p_{\rm i}}{p_{\rm f}} \right)^{1/\Gamma} = E_{\rm i} \left(\frac{p_{\rm f}}{p_{\rm i}} \right)^{(\Gamma-1)/\Gamma}, \tag{12}$$

which can be much smaller than its initial thermal energy. The balance of the initial energy is the work done by the expanding cavity on the ICM, i.e., the shock energy. This extreme case illustrates that, in principle, there is no upper limit on the fraction of the energy from an AGN outburst that ends up in the ICM. At present, the known cavities in clusters are all weakly overpressured. However, the southwestern lobe of Cen A has a pressure that is two orders of magnitude greater than that of the surrounding, unshocked gas (Kraft et al. 2003), showing that the explosive extreme can be approached for systems in poorer environments.

At the opposite extreme, consider a cavity that is inflated gently. Its pressure would remain close to that of the surrounding ICM throughout the expansion. To the extent that the pressure also remains constant during cavity inflation, the ratio of the work done by the expanding cavity to its final thermal energy would then be $\Gamma - 1$. In practice, the pressure will generally decline as a cavity inflates and expands outward into lower pressure gas. This causes additional adiabatic energy loss, boosting the ratio of the work done to its final thermal energy.

The main conclusion here is that work done by an expanding cavity is rarely less than its thermal energy and may be considerably greater. This is broadly consistent with findings for observed clusters, that the cavity enthalpy is comparable to the energy required to drive the shocks (McNamara et al. 2005; Nulsen et al. 2005b). This argument also shows that the relative energies contain information about the history of outbursts.

5.5 Distribution of AGN Heating within a Cluster

Ignoring all dissipation, we can use conservation of energy to estimate the radial dependence of the amplitude of sound waves and weak shocks,

$$\frac{\delta p}{p} \propto \rho^{-1/2} T^{-3/4} R^{-1}, \tag{13}$$

where $\rho(R)$ and $T(R)$ are the density and temperature of the ICM, and R is the radius. With this scaling, the ratio of weak shock (Equation 10) to sound heating rate (Equation 11) almost invariably decreases with radius (Fabian et al. 2005). As might be expected, this arises because the shock heating rate is more sensitive to $\delta p/p$, which decreases with the radius. The radial temperature gradient that typifies cool cores (e.g., Allen et al. 2001) probably decreases the ratio further, as the transport coefficients increase with radius.

Because Equation 13 assumes that energy is conserved, it only applies after the expanding radio lobes stop driving the pressure disturbance, i.e., after the disturbance separates from the cavities. Using it to extrapolate to small R would overestimate the relative strength of the disturbance there. The assumption of spherical symmetry, which is adequate at large distances from the radio lobes, also fails at radii smaller than the lobe separation, where the off-center energy deposition must be taken into account.

The ratio of cavity heating (Equation 9) to shock heating rate (Equation 10) is proportional to $v_{\rm K}^2 \rho^{3/2-1/\Gamma} T^{5/4-1/\Gamma} \propto \rho^{3/2-1/\Gamma} T^{9/4-1/\Gamma}$, where the Kepler speed is $v_{\rm K} = \sqrt{gR}$ and g is the acceleration due to gravity, and the ICM is assumed to be hydrostatic. The second form relies on the further approximation, $v_{\rm K}^2 \propto T$. The relatively gentle temperature rise with radius in cool cores is insufficient to offset the density decrease, so that this is generally a decreasing function of the radius (for reasonable values of Γ). Thus, cavity heating is more centrally concentrated than weak shock heating. As noted above (Section 5.1), although it is formally the most centrally concentrated of these three heating processes, cavity heating is ineffective inside the radius where the cavities are formed. Thus, weak shock heating is likely to be the most significant heating process closest to the AGN. Cavity heating probably takes over this role immediately outside the region where the radio lobes are formed (Voit & Donahue 2005).

If AGN outbursts deposit comparable amounts of energy in shocks and cavity enthalpy, then the reasoning of this section suggests that the dominant mode of AGN heating changes with radius. Closest to the AGN, weak shocks (or, possibly, sound dissipation) are likely to be most significant. Note that weak shock heating can plausibly stop the innermost gas from cooling in M87 (Section 5.2). The total rate of shock heating may not be large (Fabian et al. 2005), but because the gas closest to the nuclear black hole is the most likely to be accreted, the heating process at work on that gas plays a critical role in any AGN feedback cycle. Cavity heating may well take over beyond the radius where the radio lobes are formed. On larger scales, sound damping may become the dominant AGN heating process. On even larger scales, thermal conduction can play the dominant role in the hotter clusters. In short, it appears likely that no single AGN heating process is the most significant. It may also be that AGN heating does not act alone to prevent copious gas deposition and star formation.

5.6 Energy Injection by Radio Jets

In order to understand the process of AGN feedback, it is necessary to understand how AGN outbursts are fueled and triggered (Section 7.3), as well as the spatial distribution and form of the energy deposited by jets (e.g., Omma & Binney 2004). Observations of shocks and cavities created by AGN outbursts have motivated the development of increasingly sophisticated simulations of the interaction of jets with the ICM. Vernaleo & Reynolds (2006) found that even a variable hydrodynamic jet flowing into a static atmosphere is incapable of tranferring a significant fraction of its energy to the atmopshere. In order to avoid channeling jet energy beyond the halo, some additional physics is required.

A recent jet simulation by Heinz et al. (2006) is situated in a cluster atmosphere drawn from a realistic simulation of heirarchical structure formation. The simulated atmosphere includes the ongoing effects of cosmological evolution, such as merger shocks and turbulence. The jet also wobbles, simulating a dentist drill effect that is thought to result from instabilities along the jet (Scheuer 1974). Rather than punching through the atmosphere, the jet deposits much of its energy into gas close to the AGN. This produces a fairly realistic simulation of Cygnus A (Figure 11). Simulations of this sophistication need to be coupled with a realistic model for fueling and triggering outbursts in order to fully test feedback models.

Although radio jets appear to be the main route by which AGN energy is

conveyed to the hot gas in nearby galaxies and clusters, AGN outbursts produce uncollimated winds and intense radiation that can also heat the gas. Powerful, uncollimated nuclear winds should couple strongly to the surrounding gas, making them an effective means of heating. However, they do not appear to be a major route for AGN energy injection in nearby systems (e.g., Krongold et al. 2007). Photoionization and inverse Compton heating can also couple a small fraction of the energy radiated in an AGN outburst to the hot ISM (Ciotti & Ostriker 2001; Sazonov et al. 2005). Among other things, the significance of this process depends on the relative values of the gas temperature and the Compton temperature of the AGN radiation ($\sim$ 2 keV; Sazonov et al. 2005), making it most effective in lower temperature systems during the quasar era. Again, there is no evidence of such heating in nearby systems.

6 HEATING WITHOUT FEEDBACK

6.1 Conduction

Whether or not thermal conduction is an effective heating agent has been a controversial issue for decades. Plenty of thermal energy is available in the outskirts of clusters to heat the cores. The controversy concerns whether and how it can be effectively tapped. Assuming the magnetic fields threading clusters are tangled (Section 1.4), the conductivity is suppressed below the classical Braginskii value, inhibiting inward heat flux (Section 1.5). The magnetic field topology is not observable, so thermal conduction is poorly understood. Apart from the difficulties of maintaining local equilibrium between conductive heating and radiation (the fine-tuning problem; Stewart et al. 1984; Malagoli et al. 1987; Bregman & David 1988), there are several clusters where heat conduction cannot balance cooling throughout the core, even at the full Braginskii rate (Zakamska & Narayan 2003; Voigt & Fabian 2004; Wise et al. 2004).

On the other hand, if the thermal conductivity is only mildly suppressed (Section 1.5), conduction may be effective in the outer reaches of the cooling regions of clusters (Narayan & Medvedev 2001; Zakamska & Narayan 2003; Voigt & Fabian 2004; Wise et al. 2004), which can substantially reduce the power required from AGN heating. The heat flux depends strongly on temperature, as $\sim T^{5/2}$, so it is less important in lower temperature systems, including gE galaxies.

Dolag et al. (2004) investigated the effect of including thermal conduction in numerical simulations of galaxy cluster formation. With the thermal conductivity set to one third of the Braginskii value, they found that although the temperature structure of the ICM is significantly modified, the fraction of baryons that cools and turns into stars is little affected. This supports the argument that thermal conduction acting alone does not explain why star formation is inhibited in cluster cores.

6.2 Other Heating Mechanisms

Many mechanisms have been proposed to prevent gas from cooling to low temperatures at the centers of cooling flows, but very few of these involve feedback (e.g., Fabian 1994). As discussed in Section 4.1, without feedback it is difficult to account for the many clusters with short central cooling times. Nevertheless, such mechanisms could significantly reduce the demands on AGN heating. Most

other mechanisms that have been proposed to stop the gas from cooling rely on the energy available from mergers or, more generally, cluster binding energy (cf. Blandford 2003). Preventing the core gas from cooling in a system like the Perseus cluster requires $\sim 10^{62}$ erg over a Hubble time. Because a major merger releases $\sim 10^{64}$ ergs, only a small part of that energy needs to be tapped in order to prevent gas from cooling and forming stars. Set against this, cool cores occupy a small fraction, ~ 0.001, of the total cluster volume, presenting a relatively small target for undirected heating. Furthermore, the stably stratified cluster atmosphere, which resists the inward propagation of turbulence, combined with high central pressure (density), tends to shield the central gas from disturbances in the more tenuous gas that inhabits the bulk of a cluster.

Simulations show that major mergers can disrupt some cluster cooling flows although, even for head-on mergers, the effect need not be long lasting (e.g., Gomez et al. 2002). Higher merger rates may explain the reduced fraction of bright clusters with strong central X-ray peaks at $z > 0.5$ (Vikhlinin et al. 2007). The processes that make cooling flow clusters different from clusters with long central cooling times are still the subject of debate (e.g., McCarthy et al. 2004; O'Hara et al. 2006), but it seems likely that merger history plays some role. Thermal conduction should make it very difficult to re-establish cooling cores in hot clusters, unless it is suppressed by a large factor (Section 1.5).

Simulations of the growth of structure consistently find that the ICM should be turbulent, with typical turbulent velocities ~ 100 km s^{-1} (e.g., Kravtsov et al. 2005). Dissipation of turbulence could be a significant source of heating. Outflows from central AGN may create a similar level of turbulence, as suggested by observations of the Perseus cluster (Churazov et al. 2004), so that the source of turbulence in cool cores is unclear. Dennis & Chandran (2005) used a semiempirical model to argue that a combination of thermal conduction, turbulent dissipation, and turbulent diffusion could balance radiative losses for turbulent velocities in the range 100 - 300 km s^{-1}. However, their model does not explain why the turbulence should have the spatial distribution or power required to balance radiative losses locally.

7 FEEDBACK AND GALAXY FORMATION

7.1 Star Formation in cD Galaxies

Brightest clusters galaxies (which we refer to for convenience as cD galaxies), with masses upward of $\sim 10^{12}$ M$_\odot$ and with halos extending hundreds of kiloparsecs into the surrounding cluster, are the largest and most luminous galaxies in the Universe (Sarazin 1988). cDs are similar in appearance to gE galaxies, but there are significant differences. Their central surface brightnesses tend to be lower, their velocity dispersions rise less steeply with increasing luminosity, and they often possess stellar envelopes that lie above the $R^{1/4}$ law profiles that characterize gE galaxies. Their locations at the centers of clusters suggest they grew to such enormous sizes by swallowing stars and gas from neighboring galaxies through mergers and stripping (Gallagher & Ostriker 1972; Merritt 1985). This process is augmented at late times by the accretion of intracluster gas (Cowie & Binney 1977; Fabian & Nulsen 1977).

The stellar populations of most cDs are metal rich and dormant, and they rarely show optically active nuclei. Only 10% of optically selected cDs in non-

cooling flow clusters harbor nuclear emission line fluxes above an equivalent width of a few angstroms (Best et al. 2006; Edwards et al. 2007). In comparison, 20% of galaxies lying outside of cluster cores (Best et al. 2006) have detectable line emission, suggesting that the gas processes driving emission line activity in most galaxies are suppressed in cluster cores. The detection rate and strength of nebular emission in cD galaxies rises dramatically, to at least 45%, in cooling flow clusters (Crawford et al. 1999; Edwards et al. 2007). These emission line systems often extend tens of kiloparsecs from the nucleus (Heckman et al. 1989). They appear to be powered by a combination of shock heating, stellar photoionization, and irradiation by the surrounding X-ray gas, but rarely by photoionization from an AGN. At least half of these systems are experiencing star formation (e.g., Johnstone et al. 1987; McNamara & O'Connell 1989), and the nebular clouds and sites of star formation are usually embedded in pools of 10^9 – 10^{11} $M_\odot$ of atomic and molecular gas (e.g., Edge 2001). The ratio of young stars to galaxy mass is typically only $\sim 10^{-3}$. The corresponding star formation rates are typically a few $M_\odot$ year^{-1}, but in extreme cases they approach or exceed 100 $M_\odot$ year^{-1} (e.g., Crawford et al. 1999; McNamara et al. 2006). Young stellar population masses of 10^8 $M_\odot$ to 10^{10} $M_\odot$ are found in these systems. The largest starbursts rival those observed during the most rapid period of galaxy growth at $z = 2$ – 3 (Juneau et al. 2005). Many cDs experiencing star formation are also experiencing powerful AGN outbursts. An example of star formation in the Abell 1795 cD is shown in figure 12 from O'Dea et al. (2004).

There are two schools of thought regarding the origin of this star formation, its accompanying cold gas and nebular emission: accretion through mergers (e.g., Holtzman et al. 1992), or cooling flows (Fabian 1994). Mergers are an appealing mechanism because they are the principal route to the growth of structure in the context of the cold dark matter cosmogony, and they are an established and effective mechanism for triggering star formation in galaxies. Moreover, they provided a plausible alternative to classical cooling flows, that predict excessive star formation rates in cD galaxies (Fabian 1994). Just how effective mergers are at stimulating star formation in cluster cores in general and cDs in particular is unclear. Gas rich donor galaxies rarely inhabit the cores of clusters, perhaps because their gas becomes vulnerable to stripping long before they are able to reach the center. Furthermore, galaxies in the cores of clusters are less likely to host star formation and nuclear activity than galaxies in other environments (Best et al. 2007), which augurs against merger induced star formation. When star formation is observed in cDs, with rare exceptions, it is centered on a cooling flow. Most importantly, star formation rates approach or agree with the upper limits on cooling rates from XMM-Newton and Chandra (McNamara et al. 2004; Hicks & Mushotzky 2005; Rafferty et al. 2006; Salomé et al. 2006). The velocity structure of the cold gas fueling star formation is also consistent with having recently condensed from a static atmosphere (Jaffe et al. 2005; Salomé et al. 2006).

The emerging consistency between star formation and cooling rates is noteworthy in the broader context of galaxy formation. The mechanism suppressing cooling flows and regulating the growth of cD and gE galaxies may also be responsible for the exponential decline in the luminosity function of bright galaxies, and perhaps the relationship between bulge luminosity and black holes (e.g., Benson et al. 2003). The possibility that these two fundamentally important properties of galaxies may be explained using a single mechanism has led to the development of new galaxy formation models that incorporate AGN feedback.

Cooling flows should be relatively clean examples of galaxy and supermassive black hole growth through the accretion of cooling gas in large halos.

7.2 Galaxy Formation Models

Based on the Millennium Run dark matter simulation, Croton et al. (2006) modeled the formation and evolution of galaxies and their supermassive black holes in a concordance CDM cosmology. Their model combined numerical and semi-analytic techniques, with the goal of understanding the effects of AGN feedback on galaxies of different masses. In this model, the AGN is powered by continuous accretion, scaling in proportion to the supermassive black hole and hot gas masses divided by the Hubble time. In keeping with earlier work, they follow galaxies through a "quasar mode" of halo merging and gas accretion that leads to rapid bulge and black hole growth at $z = 2 - 3$. This is followed by a more quiescent "radio mode" that suppresses cooling flows at late times. The suppression becomes increasingly effective in more massive halos and is able to stop cooling entirely in galaxy halos with virial temperatures $T > 3 \times 10^6$ K (i.e., groups and clusters) from $z = 1$ to the present. cD galaxies continue to grow slowly at late times by dissipationless "dry mergers" lacking star formation. Radio mode feedback develops in a static hot halo driven by black hole accretion at a strongly sub-Eddington rate that adds negligibly to the black hole mass at late times. Croton et al. (2006) consider feeding the nucleus with cold cloud and Bondi accretion from the hot halos, but lacking a feedback prescription, the outcome of their model is insensitive to the mode of accretion.

Using smooth particle hydrodynamic simulations, Sijacki & Springel (2006) focused on the formation and evolution of the cD and the ICM surrounding it in the presence and absence of AGN feedback. Like Croton et al. (2006), Sijacki & Springel (2006) distinguish between major galaxy and black hole growth (BHAR model) at early times and more gentle AGN accretion and radio bubble feedback (Magorrian mode) at late times. In both the Croton et al. (2006) and Sijacki & Springel (2006) models, the correlation between black hole mass and bulge mass is imprinted during the quasar era and changes little at late times, when the suppression of cooling flows becomes important. This model assumes bubble injection repeats every 10^8 year with the energy per bubble scaling with the halo mass to the 4/3 power in the BHAR phase, and scaling with the black hole accretion rate during the Magorrian phase. In the absence of bubble heating, massive galaxies grow to unrealistically large sizes. The introduction of hot buoyant bubbles reduces cooling flows substantially, but cooling and star formation does not cease entirely at redshifts below $z = 1$. This behavior is qualitatively consistent with observations of real clusters. The Sijacki & Springel (2006) model successfully produces entropy pedestals in the cores of clusters (Voit & Donahue 2005; Donahue et al. 2006). However, their temperature and density profiles are flatter than those in real cooling flow clusters with active AGN.

These and other studies demonstrate that periodic AGN outbursts with realistic energies and duty cycles are able to suppress cooling flows and to recover the observed exponential turnover in the luminosity function of bright galaxies. They may also play a role in the development of the black hole bulge mass relation. Despite these impressive results, a great deal of the picture is missing in these simulations, including the "microphysics" of heating and of course the "macrophysics" of star formation, both of which are poorly understood. These models

also lack a working feedback prescription that reproduces the observed levels of cooling, AGN activity, and star formation in gEs and cDs at late times. They also fail to reproduce the observed temperature and density profiles of cooling atmospheres. A complete model for AGN heating should include a physically realistic treatment of the behavior of radio jets and their interaction with the ICM.

It is worth noting an important difference between the mode of energy output from AGN during the quasar epoch and present day cooling flows that is not explicitly captured in these models. Quasars are thought to be triggered by cold gas funneled onto the nucleus during halo mergers in the early Universe, leading to the rapid buildup of bulges and supermassive black holes (e.g., Blandford 1999; Springel et al. 2005). Only a small fraction of the $\sim 10^{45-46}$ erg s^{-1} of power radiated by this process must couple to the gas in order to drive an outflow capable of suppressing star formation and black hole growth. Roughly the same driving power $\sim 10^{43-45}$ erg s^{-1}, is required to offset a massive cooling flow. The enthalpy and shock energy released by cooling flow AGN, even in cDs with relatively weak radio sources, can rival the power output of a quasar. However, the bulk of the power emerging from an FR I source in a cooling flow is mechanically coupled to the gas through shocks and cavity enthalpy, and is not released as radiation. Apparently, as the specific accretion rate throttles down from the Eddington regime during the quasar era to the strongly sub-Eddington regime at late times, the power output switches from being radiation dominated to being mechanically dominated. This shift is qualitatively consistent with the observed behavior of low-mass X-ray binaries (Churazov et al. 2005).

7.3 Supermassive Black Hole Growth as a Consequence of Feedback

The demanding power requirements of the long-term suppression of cluster cooling flows by AGN should produce black holes with masses exceeding 10^9 M$_\odot$ (Fujita & Reiprich 2004). Expressing the cooling luminosity in terms of the classical cooling rate, $L_{\rm cool} = 2.5\dot{M}kT/(\mu m_{\rm H})$, multiplying by the age of the cooling flow, t, and equating to the energy released by the black hole, $\eta M_{\rm h} c^2$, gives the minimum black hole mass required to stop cooling as

$$M_{\rm h} = \frac{1.5}{\eta}\frac{s^2}{c^2}\dot{M}t \simeq 2.25 \times 10^{-4}\dot{M}t,$$

for gas cooling from 5 keV and $\eta = 0.1$. Cooling proceeding at a rate of $\dot{M} = 100$ M$_\odot$ year^{-1} since $z = 1$, which corresponds to a lookback time of $t = 7.7 \times 10^9$ year in a concordance cosmology, would form a 1.7×10^8 M$_\odot$ black hole. The power output required to quench a 1000 M$_\odot$ year^{-1} cooling flow (e.g., Abell 1835) would produce a 1.7×10^9 M$_\odot$ black hole, rivaling the largest known black hole masses. Evidently, quenching a large cooling flow over the lifetime of a galaxy cluster could produce outsized supermassive black holes in cDs, even if jet heating is efficient. NGC 1275 is one of the only cluster cooling flow cDs with a measured black hole mass. Using molecular H_2 emission line speeds, Wilman et al. (2005) measured a mass of 3×10^8 M$_\odot$. Based on the formula above, AGN feedback can quench a 150 – 200 M$_\odot$ year^{-1} cooling flow without producing an excessively massive black hole. This may leave little room for an early buildup of the black hole and subsequent long-term accretion from the cooling flow. It also requires a

relatively high efficiency for converting accreted mass to jet power if the AGN is suppressing cooling. This level of growth could cause significant departures from the established black hole mass versus bulge mass (velocity dispersion) relation extrapolated to cD galaxy luminosities (Lauer et al. 2007). Future measurements of black hole masses in cD galaxies using very large aperture telescopes (e.g., Lauer et al. 2007) will be a sensitive probe of the accretion and feedback history of clusters.

7.4 Accretion Mechanism

The accretion mechanism is a critical piece of any operational feedback loop. There are three broad categories: accretion from the hot atmosphere surrounding the black hole through the Bondi mechanism (e.g., Allen et al. 2006), accretion of cold clouds as the result of stripping or cooling blobs of gas from a cooling flow (e.g., Soker 2006), and accretion of stars (e.g., Wang & Hu 2005). The actual mechanism must operate in the sub-Eddington accretion regime, it must release most of its energy by mechanical winds or outflows and not by radiation, and it must be responsive enough to prevent cooling and heating catastrophes.

Bondi accretion, with a rate that scales as $n_{\rm e}T^{-3/2}$, is simple, natural, and in principle easy to regulate (e.g., Churazov et al. 2002). The local atmosphere responds to AGN heating by expanding, which lowers the local gas density and the accretion rate along with it. As the gas radiates away its energy, the atmosphere contracts and compresses, and the accretion rate rises. For $\gamma = 5/3$, the Bondi accretion rate depends on gas properties only through the entropy, which is affected directly by heating and cooling. The accretion rate depends on the square of the black hole mass and properties of the atmosphere within the radius of influence of the black hole, all of which are difficult or impossible to measure with current instrumentation. Bondi accretion appears to be energetically plausible in lower luminosity gE galaxies (Allen et al. 2006), but is probably unable to power the largest outbursts in clusters of galaxies (Rafferty et al. 2006).

Ample supplies of cold gas are available in cDs to fuel the AGN. If this gas were supplied by stripping or mergers, it would arrive sporadically in a manner unrelated to the properties of the cooling atmosphere. This makes the accretion rate difficult to tune, unless the gas is stored in a disk, which is somehow regulated in the vicinity of the black hole. Gas cooling out of the ICM would naturally be subject to thermostatic control by periodic outbursts (e.g., Soker 2006). Even so, understanding how energy emerging from a region smaller than the size of the solar system is able to regulate flows on the vast scales of clusters is a monumental challenge.

7.5 Observational Constraints on Feedback Models

We pointed out earlier that the conditions in the cores of clusters lend themselves to detailed study of the rudiments of galaxy formation. Because the entire cycle of heating, cooling, feedback, and star formation can be explored there in great detail, cooling flows provide a standard against which models of galaxy formation (e.g., Sijacki & Springel 2006) can be tested. These models should satisfy the following conditions:

1. A small fraction, $\lesssim 10\%$, of cDs at $z \sim 0$ are experiencing star formation perhaps as a consequence of the inability of AGN to balance radiative cool-

ing at all times from their dense, $\sim 10^{-1}$ cm^{-3}, atmospheres with cooling times $\ll 10^9$ year. Infall of cold gas by mergers or stripping is another potential source of cold gas. However, it might be difficult to understand why stripping occurs preferentially in the cores of clusters with short cooling times.

2. In both gEs and cDs, AGN heating scales in proportion to the cooling luminosity, as expected in an operational feedback loop. It is not clear whether or how the level of feedback scales with black hole mass or halo mass.
3. Bondi accretion may power the AGN in gEs (Allen et al. 2006) but is probably unable to do so in more massive cD galaxies. Only the most powerful cluster outbursts require accretion rates approaching ~ 1 M$_\odot$ year^{-1}; typical rates are $\sim 10^{-2}$ M$_\odot$ year^{-1}, which is a small fraction of the Eddington accretion rate of a 10^8 M$_\odot$ black hole.
4. The jet model most directly associated with the Magorrian mode of Sijacki & Springel (2006) and the radio mode of Croton et al. (2006) must account for the enormous range in radiative efficiency and large jet kinetic energy observed in cDs. It should also recover the observed temperature, density, and entropy profiles in the cores of clusters (Borgani 2004; Voit & Donahue 2005).
5. The existence of very powerful AGN outbursts and the persistent energy demands of cooling imply substantial black hole growth at late times in cD galaxies. There is tantalizing new evidence that cDs and their central black holes grow at an average rate that crudely follows the slope of the black hole mass versus bulge mass relation (Häring & Rix 2004) once star formation is taken into account (Rafferty et al. 2006). However, bulges and black holes do not always grow in lockstep. Other lines of evidence suggest that the slope flattens in cD galaxies (Lauer et al. 2007).
6. Star formation parameterized with a Schmidt-Kennicutt law is probably a reasonable approximation in these systems (e.g., Egami et al. 2006; McNamara et al. 2006), although this issue is in need of further study. Disk formation, which is a staple of semianalytic galaxy formation models, is rare or short-lived (e.g., Heckman et al. 1989; Salomé et al. 2006). Energy pumped into the hot gas by starburst winds, $\lesssim 10^{43}$ erg s^{-1}, is negligible on the scale of the cooling flow (McNamara et al. 2004, 2006), but may be important near the nucleus of the cD where fueling of the AGN is actively occurring.
7. Finally, the observed level and spatial distribution of chemical enrichment, and abundance ratios in the hot gas must constrain the history of star formation in the cores of clusters and the level of mixing generated by AGN outbursts and mergers.

8 CONCLUDING REMARKS

The editors of Discover Magazine's Winter 2007 special issue "Unseen Universe" posed the following question to Martin Rees: "Is there any particular image that you saw recently that reminded you anew of just how much progress we've made?" Rees's response provides a succinct history of this field. "I've been especially impressed by the X-ray images of galaxy clusters which are now becoming available from the Chandra satellite and other instruments. We see gas being churned up

by explosions and huge black holes in the center of the cluster. We see how it's cooling down and how the cooling is being balanced by tremendous outbursts of jets and bubbles of hot gas. This is something that most people didn't suspect was happening until these images revealed it."

If many people did not suspect this was happening before Chandra revealed it, why not? The Rosat observatory had already established that radio sources are interacting with the hot gas surrounding them (Böhringer et al. 1993; Carilli et al. 1994), and it had been pointed out previously that AGN (e.g., Pedlar et al. 1990; Baum & O'Dea 1991; Owen & Eilek 1998; Tucker & David 1997; Binney & Tabor 1995) and thermal conduction (Rosner & Tucker 1989; Meiksin 1988) could offset cooling in some clusters. In our view, these solutions were not widely embraced because, like the classical cooling flow model itself, they lacked persuasive observational and theoretical support. As is often true in astronomy, the impasse was broken by new, high-resolution instrumentation. XMM-Newton spectroscopy revealed that hot gas in clusters cannot be cooling at the classical rates. At about the same time, high resolution Chandra images identified AGN feedback as the probable heating agent. But the real situation is more complicated. The data show that AGN heating is more subtle than early theoretical studies envisioned. Heating is not a violent, local process. It is gentle and spatially dispersed. There is scant evidence for constant density cores or central temperature spikes, and entropy inversions as some nuclear heating models predicted. To our knowledge, no one anticipated cool rims surrounding the cavities, ripples, ghost cavities, and quasar-like outbursts that are barely audible in the radio and optically faint in the nucleus. The data were inadequate and so was the physics.

Much remains to be done. We do not understand how jets are powered and what they are made of, how the putative feedback loop works, how efficiently jets heat the gas, and we still cannot be sure that they are the sole heating agent or even the principal one. These issues will take time to resolve, but a great deal of progress has already been made, notably in ever more realistic jet simulations (e.g., Figure 11) that can now be tested against high quality data. They must be resolved in order to understand the role of supermassive black holes in galaxy and large-scale structure formation. We conclude by listing several issues and avenues of research that we believe will lead to substantial progress in this field.

FUTURE ISSUES

1. XMM-Newton spectroscopy has excluded mass deposition at the classical rates in cooling flows. However, deposition at substantial levels comparable to observed star-formation rates have not been ruled out. A search for Fe XVII and other lines at levels that are consistent with observed star formation rates is within the grasp of XMM-Newton's reflection grating spectrometer, and will be within easy reach of a future Constellation-X. Combined with increasingly accurate star formation rates (item 5), this would constitute a strong test of new, feedback-based cooling flow models.
2. It is difficult or impossible to detect cavities and shock fronts in distant clusters and groups beyond $z \sim 0.5$. In principle, radio observations, especially at low frequencies, can probe the history of feedback and heating at earlier times. However, the large variation in radio synchrotron efficiency must first be understood and calibrated.

3. The time distribution of AGN jet power in galaxies and clusters, which is an essential part of a feedback model, is poorly understood. Existing X-ray cavity surveys are limited in size and suffer strong selection biases. A large, unbiased search for cavities and shocks in a flux or volume limited sample of groups and clusters is required to more accurately determine the average AGN heating rate.
4. The environmental factors that trigger AGN outbursts, particularly the most powerful ones in cD galaxies ($> 10^{61}$ erg), are poorly understood. High resolution imaging and spectroscopy of the stars and gas in nuclei of galaxies, made at a variety of wavelengths, will characterize the properties of nuclear gas disks, stellar cusps, and cores. This knowledge should provide a deeper understanding of the accretion and feedback process, and hopefully new insight as to why many systems are as powerful as quasars and yet they don't reveal themselves as such. Most importantly, measurements of black hole masses in cD galaxies using future large aperture telescopes will place restrictive limits on the history of AGN feedback in clusters.
5. Limits on the rate of cooling in the cores of galaxies and clusters have become tight enough to warrant better measurements of star formation rates and histories. This will require precision photometry over a broad passband (UV to far IR) and careful accounting for dust and positive feedback from radio triggered star formation (De Young 1995; O'Dea et al. 2004; see Figure 12). Combining this information with black hole growth rates estimated from cavities and shock fronts will yield new insight into how bulges and supermassive black holes grow at late times.
6. New high fidelity jet models (e.g., Heinz et al. 2006 see Figure 11) combined with sensitive X-ray measurements of cavities and shock fronts will increase our understanding of jet dynamics, energetics, content, radiative efficiencies, and ultimately how jets form. The form of energy deposition by jets is a critical component of any feedback model.
7. Models are needed for the fueling and triggering of AGN outbursts, including the part played by mergers.
8. How cavity enthalpy and weak shock energy is dissipated, how efficiently it heats the gas, and where the heat is deposited are fundamentally important questions that have not been satisfactorily answered.
9. The contribution of AGN outbursts to deviations from the expected scaling relationships between mass, temperature, and X-ray luminosity of clusters (e.g., O'Hara et al. 2006; Gitti et al. 2007) is poorly understood. The energy required to quench a large cooling flow over its lifetime is comparable to the 1 keV per baryon necessary to preheat a cluster. AGN may contribute significantly to preheating.

ACKNOWLEDGEMENTS

We thank David Rafferty and Laura Bîrzan for helpful discussions and for providing figures. Michael Balogh read the draft in a primitive state of development and offered helpful comments. Thanks to Hans Böhringer, Larry David, Bill Forman, Dan Harris, Christine Jones, Maxim Markevitch, and Alexey Vikhlinin for their advice. We thank Chris O'Dea, Sebastian Heinz, and Marcus Brüggen

for permission to print figures from their work. We especially thank our friend and collaborator Michael Wise, one of the pioneers of this field, who has helped to shape our thoughts on this topic. B.R.M. was supported in part by NASA Long Term Space Astrophysics grant NAG5-11025. P.E.J.N. acknowledges NASA grant NAS8-01130.

References

Allen SW, Schmidt RW, Fabian AC. 2001. *MNRAS* 328:L37-41

Allen SW, Schmidt RW, Ebeling H, Fabian AC, van Speybroeck L. 2004. *MNRAS* 353:457-467

Allen SW, Dunn RJH, Fabian AC, Taylor GB, Reynolds CS. 2006. *MNRAS* 372:21-30

Arnaud M. 2005. In Background Microwave Radiation and Intracluster Cosmology, ed. F Melchiorri, Y Rephaeli, pp. 77-116. Netherlands: IOS Press

Arnaud M, Evrard AE. 1999. *MNRAS* 305:631-640

Arnaud M, Rothenflug R, Boulade O, Vigroux L, Vangioni-Flam E. 1992. *Astron. Astrophys.* 254:49-64

Balbus SA, Soker N. 1989. *Astrophys. J.* 341:611-630

Babul, A., Balogh, M. L., Lewis, G. F., & Poole, G. B. 2002, *MNRAS* , 330, 329

Baum SA, O'Dea CP. 1991. *MNRAS* 250:737-749

Baumgartner WH, Loewenstein M, Horner DJ, Mushotzky RF. 2005. *Astrophys. J.* 620:680-696

Begelman MC. 2001. In *ASP Conf. Proc. 240: Gas and Galaxy Evolution,* ed. JE Hibbard, M Rupen, JH van Gorkom, p363. San Francisco: ASP

Begelman MC. 2004. Coevolution of Black Holes and Galaxies, from the Carnegie Observatories Centennial Symposia, LC Ho ed. Carnegie Observatories Astrophysics Series:CUP p 374

Begelman MC, Blandford RD, Rees MJ. 1984. Reviews of Modern Physics 56:255-351

Benson AJ, Bower RG, Frenk CS, Lacey CG, Baugh CM, Cole S. 2003. *Astrophys. J.* 599:38-49

Best PN, Kaiser CR, Heckman TM, Kauffman G. 2006. *MNRAS* 368:L67-70

Best PN, von der Linden A, Kauffmann G, Heckman TM, Kaiser CR. 2007. *MNRAS* in press

Binney J, Tabor G. 1995. *MNRAS* 276:663-678

Binney J, Bibi A, Omma H. 2007. *MNRAS* 377:142-146

Bîrzan L, Rafferty DA, McNamara BR, Wise MW, Nulsen PEJ. 2004. *Astrophys. J.* 607:800-809

Blandford RD. 1999. In Galaxy Dynamics, ed. DR Merritt, M Valuri, JA Sellwood, pp. 87-95. San Francisco: ASP

Blandford RD. 2003. In High Energy Processes and Phenomena in Astrophysics, ed. XD Li, V Trimble, and ZR Wang, pp. 3-22. San Francisco: ASP

Blandford RD, Rees MJ. 1974. *MNRAS* 169:395-415

Blanton EL, Sarazin CL, McNamara BR, Wise MW. 2001. *Astrophys. J.* 558:L15-19

Blanton EL, Sarazin CL, McNamara BR. 2003. *Astrophys. J.* 585:227-243

Böhringer H, Morfill GE. 1988. *Astrophys. J.* 330:609-619

Böhringer H, Voges W, Fabian AC, Edge AC, Neumann DM. 1993. *MNRAS* 264:L25-L28

Böhringer H, Matsushita K, Churazov E, Ikebe Y, Chen Y. 2002. *Astron. Astrophys.* 382:804-820

Böhringer H, Schuecker P, Pratt GW, Finoguenov A, eds. 2007. Proc. of Heating versus Cooling in Galaxies and Clusters of Galaxies. Garching: Springer-Verlag

Borgani S 2004, APS&S, 294, 51

Braginskii SI. 1965. Rev. Plasma Phys. 1:205-311

Branduardi-Raymont G, Fabricant D, Feigelson E, Gorenstein P, Grindlay J, Soltan A, Zamorani G. 1981. *Astrophys. J.* 248:55-60

Bregman JN, David LP. 1988. *Astrophys. J.* 326:639-644

Bregman JN, Fabian AC, Miller ED, Irwin JA. 2006. *Astrophys. J.* 642:746-51

Brighenti F, Mathews WG. 2003. *Astrophys. J.* 587:580-588

Brüggen M. 2002. *Astrophys. J.* 571:L13-L16

Brüggen M, Kaiser CR. 2001. *MNRAS* 325:676-684

Brüggen M, Kaiser CR. 2002. *Nature* 418:301-303

Brüggen M, Ruszkowski M, Hallman E. 2005. *Astrophys. J.* 630:740-749

Burbidge G. 1956. *Astrophys. J.* 124:416-429

Burns JO. 1990. *Astron. J.* 99:14-30

Canizares CR, Clark GW, Jernigan JG, Markert TH. 1982. *Astrophys. J.* 262:33-43

Canizares CR, Markert TH, Donahue ME. 1988. NATO ASIC Proc. 229: Cooling Flows in Clusters and Galaxies, 63-72

Carilli CL, Perley RA, Harris DE. 1994. *MNRAS* 270:173-177

Carilli CL, Taylor GB. 2002. *Ann. Rev. Astron. Astrophys.* 40:319-348

Cavaliere A, Fusco-Femiano R. 1976. *Astron. Astrophys.* 49:137-144

Cavaliere A, Lapi A. 2006. *Astrophys. J.* 647:L5-8

Churazov E, Inogamov N. 2004. *MNRAS* 350:L52-L56

Churazov E, Brüggen M, Kaiser CR, Böhringer H, Forman W. 2001. *Astrophys. J.* 554:261-273

Churazov E, Sunyaev R, Forman W, Böhringer H. 2002. *MNRAS* 332:729-734

Churazov E, Forman W, Jones C, Sunyaev R, Böhringer H. 2004. *MNRAS* 347:29-35

Churazov E, Sazonov S, Sunyaev R, Forman W, Jones C, Boehringer H. 2005. *MNRAS* 363:L91-95

Ciotti L, Ostriker JP. 2001. *Astrophys. J.* 551:131-152

Clarke TE, Kronberg PP, Böhringer H. 2001. *Astrophys. J.* 547:L111-114

Clarke TE, Blanton EL, Sarazin CL. 2004. *Astrophys. J.* 616:178-191

Clarke TE, Sarazin CL, Blanton EL, Neumann DM, Kassim NE. 2005. *Astrophys. J.* 625:748-191

Cowie LL, Binney J. 1977. *Astrophys. J.* 215:723-732

Crawford CS, Allen SW, Ebeling H, Edge AC, Fabian AC. 1999. *MNRAS* 306:857-896

Crawford CS, Sanders JS, Fabian AC. 2005. *MNRAS* 361:17-33

Croton DJ, et al. 2006. *MNRAS* 365:11-28

Croston JH, Hardcastle MJ, Birkinshaw M. 2005. *MNRAS* 357:279-294

Croston JH, Kraft RP, Hardcastle MJ. 2007. *Astrophys. J.* 660:191-199

Dalla Vecchia C, Bower RG, Theuns T, Balogh ML, Mazzotta P, Frenk CS. 2004. *MNRAS* 355:995-1004

David LP, Nulsen PEJ, McNamara BR, Forman W, Jones C, Ponman T, Robertson B, Wise M. 2001. *Astrophys. J.* 557:546-559

Dennis TJ, Chandran BDG. 2005. *Astrophys. J.* 622:205-216

De Young DS. 1995. *Astrophys. J.* 446:521-527

De Young DS. 2001. The Physics of Extragalactic Radio Sources. Chicago: Univ. Chicago Press. 569 pp.

De Young DS. 2006. *Astrophys. J.* 648:200-208

De Grandi S, Molendi S. 2001. *Astrophys. J.* 551:153-159

De Grandi S, Molendi S. 2002. *Astrophys. J.* 567:163-177

De Young DS. 2003. *MNRAS* 343:719-24

Diehl S, Statler T. 2007. *Astrophys. J.* in press (astro-ph/0606215)

Dolag K, Jubelgas M, Springel V, Borgani S, Rasia E. 2004. *ApJL* 606:L97-L100

Donahue M, Horner DJ, Cavagnolo KW, Voit GM. 2006. *Astrophys. J.* 643:730-750

Dunn RJH, Fabian AC. 2004. *MNRAS* 355:862-873

Dunn RJH, Fabian AC. 2004. *MNRAS* 373:959-971

Dunn RJH, Fabian AC, Celotti A 2006, *MNRAS* , 372, 1741

Dunn RJH, Fabian AC, Taylor GB. 2005. *MNRAS* 364:1343-1353

Dwarakanath KS, Nath BB. 2006. *Astrophys. J.* 653:L9-12

Edge AC. 2001. *MNRAS* 328:762-782

Edge AC, Stewart GC. 1991. *MNRAS* 252:414-427

Edwards LOV, Hudson MJ, Balogh ML, Smith RJ. 2007. *MNRAS* 379:100-110

Egami E, Misselt KA, Wise MW, et al. 2006. *Astrophys. J.* 647:922-933

Enßlin TA, Heinz S. 2002. *Astron. Astrophys.* 384:L27-L30

Enßlin TA, Brüggen M. 2002. *MNRAS* 331:1011-1019

Ettori S. 2000. *MNRAS* 311:313-316

Ettori S, Fabian AC. 2000. *MNRAS* 317:L57-L59

Evrard AE, Metzler CA, Navarro JF. 1996. *Astrophys. J.* 469:494-507

Ezawa H, Fukazawa Y, Makishima K, Ohashi T, Takahara F, Xu H, Yamasaki NY. 1997. *ApJL* 490:L33-L36

Fabian AC. 1994. *Ann. Rev. Astron. Astrophys.* 32:277-318

Fabian AC, Nulsen PEJ. 1977 *MNRAS* 180:479-484

Fabian AC, Hu EM, Cowie LL, Grindlay J. 1981. *Astrophys. J.* 248:47-54

Fabian AC, Sanders JS, Ettori S, Taylor GB, et al. 2000. *MNRAS* 318:L65-L68

Fabian AC, Mushotzky RF, Nulsen PEJ, Peterson JR. 2001. *MNRAS* 321:L20-L24

Fabian AC, Celotti A, Blundell KM, Kassim NE, Perley RA. 2002. *MNRAS* 331:369-375

Fabian AC, Sanders JS, Allen SW, Crawford CS, Iwasawa K, Johnstone RM, Schmidt RW, Taylor GB. 2003. *MNRAS* 344:L43-L47

Fabian AC, Sanders JS, Crawford CS, Conselice CJ, Gallagher JS, Wyse RFG. 2003. *MNRAS* 344:L48-L52

Fabian AC, Reynolds CS, Taylor GB, Dunn RJH. 2005. *MNRAS* 363:891-896

Fabian AC, Sanders JS, Taylor GB, Allen SW, Crawford CS, Johnstone RM, Iwasawa K. 2006. *MNRAS* 366:417-428

Finoguenov A, David LP, Ponman TJ. 2000. *Astrophys. J.* 544:188-203

Finoguenov A, Jones C. 2001. *Astrophys. J.* 547:L107-L110

Finoguenov A, Matsushita K, Böhringer H, Ikebe Y, Arnaud M. 2002 *Astron. Astrophys.* 381:21-31

Forman W, Kellogg E, Gursky H, Tananbaum H, Giacconi R. 1972. *Astrophys. J.* 178:309-316

Forman W, Jones C. 1982. *Ann. Rev. Astron. Astrophys.* 20:547-585

Forman W, Nulsen P, Heinz S, Owen F, Eilek J, Vikhlinin A, Markevitch M, Kraft R, Churazov E, Jones C. 2005. *Astrophys. J.* 635:894-906

Forman W, Churazov E, Jones C, et al. 2007. *Astrophys. J.* in press (astro-ph/0604583)

Fujita Y, Reiprich TH. 2004. *Astrophys. J.* 612:797-804

Gallagher JS, Ostriker JP. 1972. *Astrophys. J.* 77:288-291

Giacconi R, Kellogg E, Gorenstein P, Gursky H, Tananbaum H. 1971. *Astrophys. J.* 165:L27-L35

Gitti M, Feretti L, Schindler S. 2006. *Astron. Astrophys.* 448:853-860

Gitti M, McNamara BR, Nulsen PEJ, Wise MW. 2007. *Astrophys. J.* 660:1118-1136

Gomez PL, Loken C, Roettiger K, Burns JO . 2002. *Astrophys. J.* 569:122-133

Govoni F. 2006. *Astron. Nachr.* 327:537-544

Govoni F, Feretti L. 2004. IJMod. Phys 13:1549-1594

Gu J, Xu H, Gu L, An T, Wang Y, Zhang Z, Wu X-P. 2007 *Astrophys. J.* 659:275-282

Gull SF, Northover KJE. 1973. *Nature* 244:80-83

Gursky H, Kellogg E, Murray S, Leong C, Tananbaum H, Giacconi R. 1971. *Astrophys. J.* 167:L81-L84

Gursky H, Schwartz DA. 1977. *Ann. Rev. Astron. Astrophys.* 15:541-568

Häring N, Rix H. 2004. *Astrophys. J.* 604:L89-L92

Harris DE, Krawczynski H. 2006. *Ann. Rev. Astron. Astrophys.* 44:463-506

Hatch NA, Crawford CS, Johnstone RM, Fabian AC. 2006. *MNRAS* 367:433-448

Heath D, Krause M, Alexander P. 2006. *MNRAS* 374:787-792

Heckman TM. 1981. *Astrophys. J.* 250:L59-L63

Heckman TM, Baum SA, van Breugel WJM, McCarthy P. 1989. *Astrophys. J.* 338:48-77

Heinz S, Reynolds C, Begelman M. 1998. *Astrophys. J.* 501:126-136

Heinz S, Choi Y-Y, Reynolds CS, Begelman MC. 2002. *Astrophys. J.* 569:L79-L82

Heinz S, Churazov E. 2005. *ApJL* 634:L141-L144

Heinz S, Bruggen M, Young A, Levesque E. 2006. *MNRAS* 373:L65-69

Hicks AK, Mushotzky R. 2005. *Astrophys. J.* 635:L9-L12

Holtzman JA, Faber SM, Shaya EJ, Lauer TR, Groth EJ, et al. 1992. *Astron. J.* 103:691-702

Huang Z, Sarazin CL. 1998. *Astrophys. J.* 496:728-736

Ikebe Y, et al. 1997. *Astrophys. J.* 481:660-672

Irwin JA Bregman JN. 2000. *Astrophys. J.* 538:543-554

Irwin JA, Bregman JN. 2001. *Astrophys. J.* 546:150-156

Jaffe W, Bremer MN, Baker K. 2005. *MNRAS* 360:748-762

Jetha NN, Ponman TJ, Hardcastle MJ. Croston JH. 2007. *MNRAS* 376:193-204

Johnstone RM, Fabian AC, Nulsen PEJ. 1987. *MNRAS* 224:75-91

Jones C, Forman W, Vikhlinin A, Markevitch M, David L, et al. 2002. *Astrophys. J.* 567:L115-118

Jones C, Forman W, Churazov E, Nulsen P, Kraft R, Murray S. 2007. See Böhringer et al.. 2007, pp. 143-152

Jones TW, de Young DS. 2005. *Astrophys. J.* 624:586-605

Juneau S, et al. 2005. *ApJL* 619:L135-L138

Kaiser CR, Pavlovski G, Pope ECD, Fanghor H. 2005. *MNRAS* 359:493-503

Kempner JC, Sarazin CL, Ricker PA. 2002. *Astrophys. J.* 579:236-246

Kochanek CS, White M, Huchra J, Macri L, Jarrett TH, Schneider SE, Mader J. 2003. *Astrophys. J.* 585:161-181

Kraft RP, Vázquez SE, Forman WR, Jones C, Murray SS, Hardcastle MJ, Worrall DM, Churazov E. 2003. *Astrophys. J.* 592:129-146

Kravtsov AV, Nagai D, Vikhlinin AV. 2005. *Astrophys. J.* 625:588-595

Kronberg PP. 2003. Astronomical Society of the Pacific Conference Series, 301:169-183

Krongold Y, Nicastro F, Elvis M, Brickhouse N, Binette L, Mathur S, Jiménez-Bailón E. 2007. *Astrophys. J.* 659:1022-1038

Landau LD, Lifshitz EM. 1987. *Course of Theoretical Physics, Vol. 6, Fluid Mechanics.* London: Pergamon

Lauer TR, et al. 2007. *Astrophys. J.* 662:808-834

Lin YT, Mohr JJ, Stanford SA. 2003. *Astrophys. J.* 591:749-763

Loewenstein M. 2006. *Astrophys. J.* 648:230-249

Lyutikov M. 2006. *MNRAS* 373:73-78

Machacek M, Nulsen PEJ, Jones C, Forman WR. 2006. *Astrophys. J.* 648:947-955

Malagoli A, Rosner R, Bodo G. 1987. *Astrophys. J.* 319:632-636

Markevitch M. 1998. *Astrophys. J.* 504:27-34

Markevitch M, Mazzotta P, Vikhlinin A, et al. 2003. *Astrophys. J.* 586:L19-L23

Markevitch M, Vikhlinin A. 2007. Physics Reports 443:1-53

Markevitch M, Forman WR, Sarazin CL, Vikhlinin A. 1998. *Astrophys. J.* 503:77-96

Mathews WG, Bregman JN. 1978. *Astrophys. J.* 224:308-319

Mathews WG, Brighenti F. 2003. *Ann. Rev. Astron. Astrophys.* 41:191-239

Mathews WG, Brighenti F. 2007. *Astrophys. J.* 660:1137-1145

Mazzotta P, Kaastra JS, Paerels FB, Ferrigno C, Colafrancesco S, et al. 2002. *Astrophys. J.* 567:L37-40

Meiksin A. 1988. *Astrophys. J.* 334:59-69

McCarthy IG, Balogh ML, Babul A, Poole GB, Horner DJ. 2004. *Astrophys. J.* 613:811-830

McNamara BR, O'Connell RW. 1989. *Astron. J.* 98:2018-2043

McNamara BR, O'Connell RW. 1993. McNamara BR, O'Connell RW. 1993. *Astron. J.* 105:417-426

McNamara BR, et al. 2000. *Astrophys. J.* 534:L135-138

McNamara BR, Wise MW, Nulsen PEJ, et al. 2001. *Astrophys. J.* 562:L149-L12

McNamara BR, Nulsen PEJ, Wise MW, Rafferty DA, Carilli C, Sarazin CL, Blanton EL. 2005. *Nature* 433:45-47

McNamara BR, Wise MW, Murray SS. 2004. *Astrophys. J.* 601:173-183

McNamara BR, Rafferty DA, Birzan L, Steiner J, Wise MW, et al. 2006. *Astrophys. J.* 648:164-175

Merritt D. 1985. *Astrophys. J.* 289:18-32

Mitchell RJ, Culhane JL, Davison PJN, Ives JC. 1976. *MNRAS* 175:29P-33P

Molendi S, Pizzolato F. 2001. *Astrophys. J.* 560:194-200

Morita U, Ishisaki Y, Yamasaki NY, Ota N, Kawano N, et al. 2006. Publ. Astron. Soc. Jpn. 58:719-742

Morris RG, Fabian AC. 2005. *MNRAS* 358:585-600

Mushotzky RF, Loewenstein M. 1997. *Astrophys. J.* 481:L63-L66

Mushotzky RF. 2004. Clusters of Galaxies: Probes of Cosmological Structure and Galaxy Evolution, 123-142

Nagai D, Vikhlinin A, Kravtsov AV. 2007. 655:98-108

Nakazawa K, Makishima K, Fukazawa Y. 2007. Publ. Astron. Soc. Jpn. in press (astro-ph/0612753)

Narayan R, Medvedev MV. 2001. *Astrophys. J.* 562:L129-L132

Nipoti C, Binney J. 2004. *MNRAS* 349:1509-1515

Nipoti C, Binney J. 2005. *MNRAS* 361:428-436

Nulsen PEJ. 1986. *MNRAS* 221:377-392

Nulsen PEJ, David LP, McNamara BR, Jones C, Forman WR, Wise M. 2002. *Astrophys. J.* 568:163-173

Nulsen PEJ, Hambrick DC, McNamara BR, Rafferty D, Birzan L, Wise MW, David LP. 2005. *Astrophys. J.* 625:L9-L12

Nulsen PEJ, McNamara BR, Wise MW, David LP. 2005. *Astrophys. J.* 628:629-636

Nulsen PEJ, Jones C, Forman WR, David LP, McNamara BR, et al. 2007. See Böhringer et al. 2007, pp. 223-28

Nusser A, Silk J, Babul A. 2006. *MNRAS* 373:739-746

O'Dea CP, Baum SA, Mack J, Koekemoer AM, Laor A. 2004. *Astrophys. J.* 612:131-151

Oegerle WR, Cowie L, Davidsen A, Hu E, Hutchings J, et al. 2001. *Astrophys. J.* 560:187-193

O'Hara TB, Mohr JJ, Bialek JJ, Evrard AE. 2006. *Astrophys. J.* 639:64-80

Omma H, Binney J. 2004. *MNRAS* 350:L13-L16

Omma H, Binney J, Bryan G, Slyz A. 2004. *MNRAS* 348:1105-1119

Owen FN, Eilek JA. 1998. *Astrophys. J.* 493:73-80

Peres CB, Fabian AC, Edge AC, Allen SW, Johnstone RM, White DA. 1998. *MNRAS* 298:416-423

Peterson JR, et al. 2001. *Astron. Astrophys.* 365:L104-L109

Peterson JR, Fabian AC. 2006. *Phys. Rep.* 427:1-39

Peterson JR, Kahn SM, Paerels FBS, Kaastra JS, Tamura T, Bleeker JAM, Ferrigno C, Jernigan JG. 2003. *Astrophys. J.* 590:207-224

Pedlar A, Ghataure HS, Davies RD, Harrison BA, Perley R, Crane PC, Unger SW. 1990. *MNRAS* 246:477-489

Piffaretti R, Jetzer P, Kaastra JS, Tamura T. 2005. *Astron. Astrophys.* 433:101-111

Pfrommer C, Enßlin TA, Sarazin CL. 2005. *Astron. Astrophys.* 430:799-810

Pizzolato F, Soker N. 2006. *MNRAS* 371:1835-1848

Pointecouteau E, Arnaud M, Kaastra J, de Plaa J. 2004. *Astron. Astrophys.* 423:33-47

Ponman TJ, Cannon DB, Navarro JF. 1999. *Nature* 397:135-137

Ponman TJ, Sanderson AJR, Finoguenov A. 2003. *MNRAS* 343:331-342

Pope ECD, Pavlovski G, Kaiser CR, Fangohr H. 2006. *MNRAS* 367:1121-1131

Quilis V, Bower RG, Balogh ML. 2001. *MNRAS* 328:1091-1097

Rafferty DA, McNamara BR, Nulsen PEJ, Wise MW. 2006. *Astrophys. J.* 652:216-231

Rebusco P, Churazov E, Bohringer H, Forman W. 2005. MNRAS 359:1041-1048

Renzini A. 2004. Clusters of Galaxies: Probes of Cosmological Structure and Galaxy Evolution, 260

Reynolds CS, Heinz S, Begelman MC. 2001. *Astrophys. J.* 549:L179-82

Reynolds CS, Heinz S, Begelman MC. 2002. *MNRAS* 332:271-282

Reynolds CS, McKernan B, Fabian AC, Stone JM, Vernaleo JC. 2005. *Astrophys. J.* 357:242-250

Rizza E, Loken C, Bliton M, Roettiger K, Burns JO, Owen FN. 2000. *Astron. J.* 119:21-31

Robinson K, et al. 2004. *Astrophys. J.* 601:621-643

Roediger E, Brüggen M, Rebusco P, Böhringer H, Churazov E. 2006. *MNRAS* 325:15-28

Rosner R, Tucker WH. 1989. *Astrophys. J.* 338:761-769

Roychowdhury S, Ruszkowski M, Nath BB, Begelman MC. 2004. *Astrophys. J.* 615:681-688

Ruszkowski M, Begelman MC. 2002. *Astrophys. J.* 581:223-228

Ruszkowski M, Brüggen M, Begelman MC. 2004a. *Astrophys. J.* 611:158-163

Ruszkowski M, Brüggen M, Begelman MC. 2004b. *Astrophys. J.* 615:675-680

Salomé P, Combes F, Edge AC, Crawford C, Erlund M, et al. 2006. å454:437-445

Sanders JS, Fabian AC, Dunn,RJH. 2005. *MNRAS* 360:133-140

Sanders JS, Fabian AC, Allen SW, Schmidt RW. 2004. *MNRAS* 349:952-972

Sarazin CL. *X-ray Emission from Clusters of Galaxies.* Cambridge: Cambridge University Press

Sazonov S Yu, Ostriker JP, Ciotti L, Sunyaev RA. 2005. *MNRAS* 358:168-180

Schindler S, Castillo-Morales A, De Filippis E, Schwope A, Wambsganss J. 2001. å376:L27-30

Serlemitsos PJ, Smith BW, Boldt EA, Holt SS, Swank JH. 1977. *Astrophys. J.* 211:L63-L66

Scheuer PAG. 1974. *MNRAS* 166:513-528

Siemiginowska, A., Cheung, C. C., LaMassa, S., Burke, D. J., Aldcroft, T. L., Bechtold, J., Elvis, M., & Worrall, D. M. 2005, *Astrophys. J.* , 632, 110

Sijacki D, Springel V. 2006. *MNRAS* 366:397-416

Silk J. 1976. *Astrophys. J.* 208:646-649

Smith DA, Wilson AS, Arnaud KA, Terashima Y, Young AJ. 2002. *Astrophys. J.* 565:195-207

Soker N, Blanton EL, Sarazin CL. 2002. *Astrophys. J.* 573:533-541

Soker N. 2006. New Astron. 12:38-46

Spergel DN, Bean R, Doré O, Nolta MR, Bennett CL, et al. 2007. *Astrophys. J. Suppl.* 170:377-408

Spitzer L. 1962. *Physics of Fully Ionized Gases.* New York: Interscience

Springel V, Di Matteo T, Hernquist L. 2005. *MNRAS* 361:776-794

Stewart GC, Fabian AC, Nulsen PEJ, Canizares CR. 1984. *Astrophys. J.* 278:536-543

Tamura T, et al. 2001. *Astron. Astrophys.* 365:L87-L92

Tamura T, Kaastra JS, den Herder JWA, Bleeker JAM, Peterson JR. 2004. *Astron. Astrophys.* 420:135-146

Tribble PC. 1989. *MNRAS* 238:1247-1260

Tucker W, David LP. 1997. *Astrophys. J.* 484:602-607

Vallée JP. 2004. New Astronomy Review 48:763-841

Vernaleo JC, Reynolds CS. 2006. *Astrophys. J.* 645:83-94

Vikhlinin A, Markevitch M, Forman W, Jones C. 2001. *Astrophys. J.* 555:L87-L90

Vikhlinin A, Markevitch M, Murray SS. 2001. *ApJL* 549:L47-L50

Vikhlinin A, Markevitch M, Murray SS, Jones C, Forman W, Van Speybroeck L. 2005. *Astrophys. J.* 628:655-672

Vikhlinin A, Kravtsov A, Forman W, Jones C, Markevitch M, Murray SS, Van Speybroeck L. 2006. *Astrophys. J.* 640:691-709

Vikhlinin A, Burenin R, Forman W, Jones C, Hornstrup A, et al. 2007. See Bohringer et al. 2007, pp. 48-53

Voigt LM, Fabian AC. 2004. *MNRAS* 347:1130-1149

Voit GM. 2005. Reviews of Modern Physics, 77:207-258

Voit GM, Donahue M. 2005. *Astrophys. J.* 634:955-963

Wang J-M, Hu C. 2005. *Astrophys. J.* 630:L125-L128

Wilman RJ, Edge AC, Johnstone RM. 2005. *MNRAS* 359:755-764

Wise MW, McNamara BR, Murray SS. 2004. *Astrophys. J.* 601:184-196

Wise MW, McNamara BR, Nulsen PEJ, Houck JC, David LP. 2007. *Astrophys. J.* 659:1153-1158

Wu KKS, Fabian AC, Nulsen PEJ. 2000. *MNRAS* 318:889-912

Young AJ, Wilson AS, Mundell CG. 2002. *Astrophys. J.* 579:560-570

Zakamska NL, Narayan R. 2003. *Astrophys. J.* 582:162-169

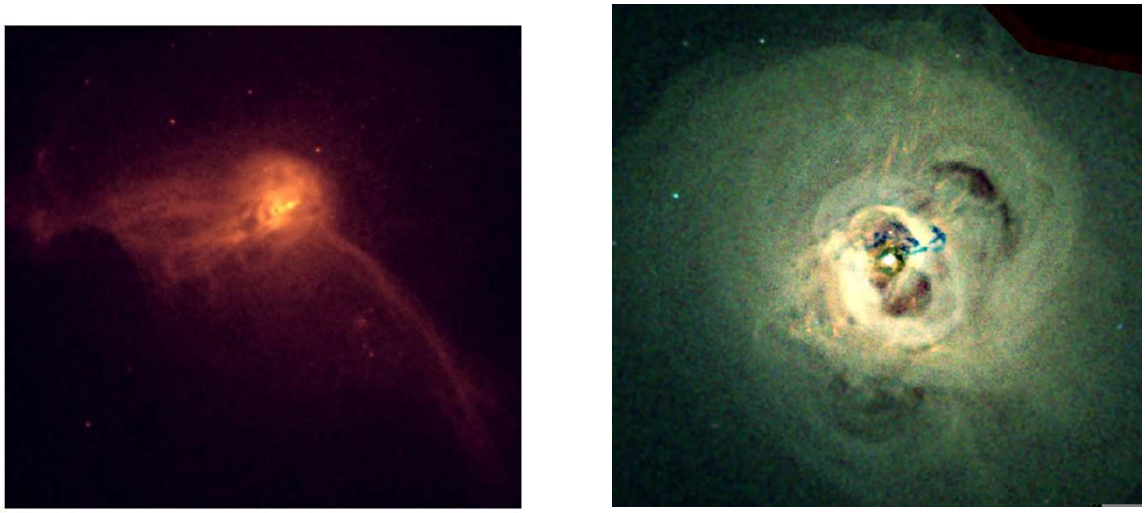

Figure 1: *Left.* Chandra X-ray image of M87 showing structure in the hot gas associated with the AGN outburst (Forman et al. 2007). Several small cavities and filaments of uplifted gas are visible. X-ray emission from the radio jet is seen at the center. *Right.* Chandra X-ray image of the Perseus cluster exposed for 900,000 s from Fabian et al. (2006). Two inner cavities containing the active radio lobes and two outer ghost cavities are seen. The sound waves (weak shocks) are visible as a series of circular ripples surrounding the cavities. The central blue structure is absorption by a foreground galaxy.

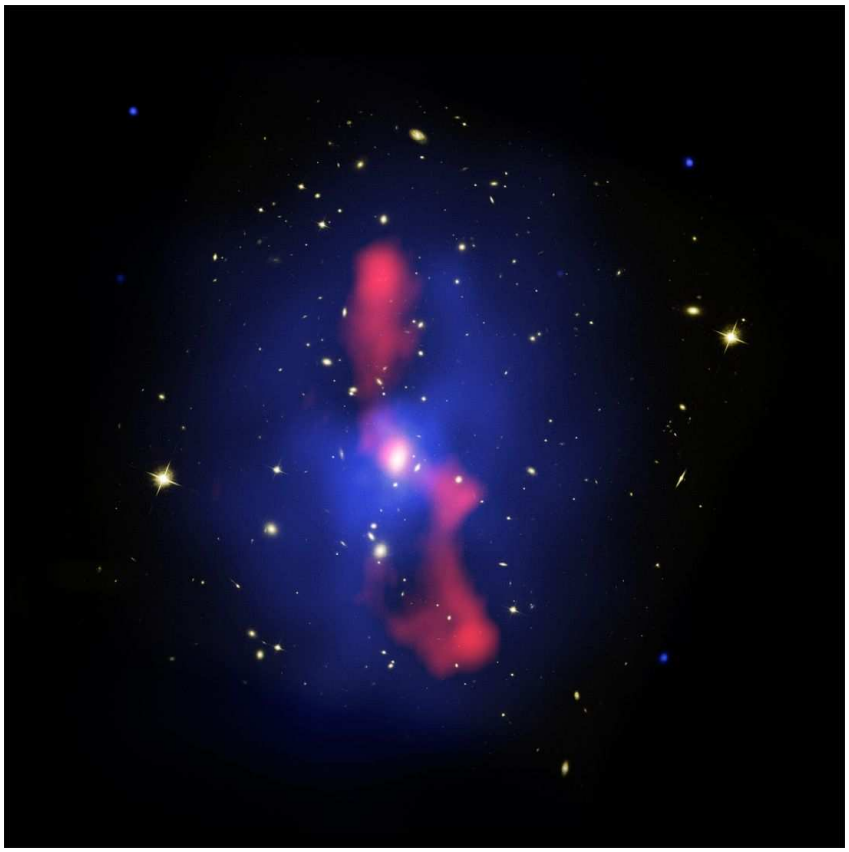

Figure 2: Hubble Space Telescope visual image of the MS0735.6+7421 cluster superposed with the Chandra X-ray image in blue and a radio image from the Very Large Array at a frequency of 330 MHz in red. The X-ray image shows an enormous pair of cavities, each roughly 200 kpc in diameter that are filled with radio emission. The radio jets have been inflating the cavities for 10^8 years with an average power of $< 2{\times}10^{46}$ erg s^{-1}. The displaced gas mass is $< 10^{12}$ M$_\odot$. The cavities and radio source are bounded by a weak shock front. The cavities are well outside the central galaxy and cooling region of the cluster. The supermassive black hole grew by at least $< 3 \times 10^8$ M$_\odot$ during the outburst.

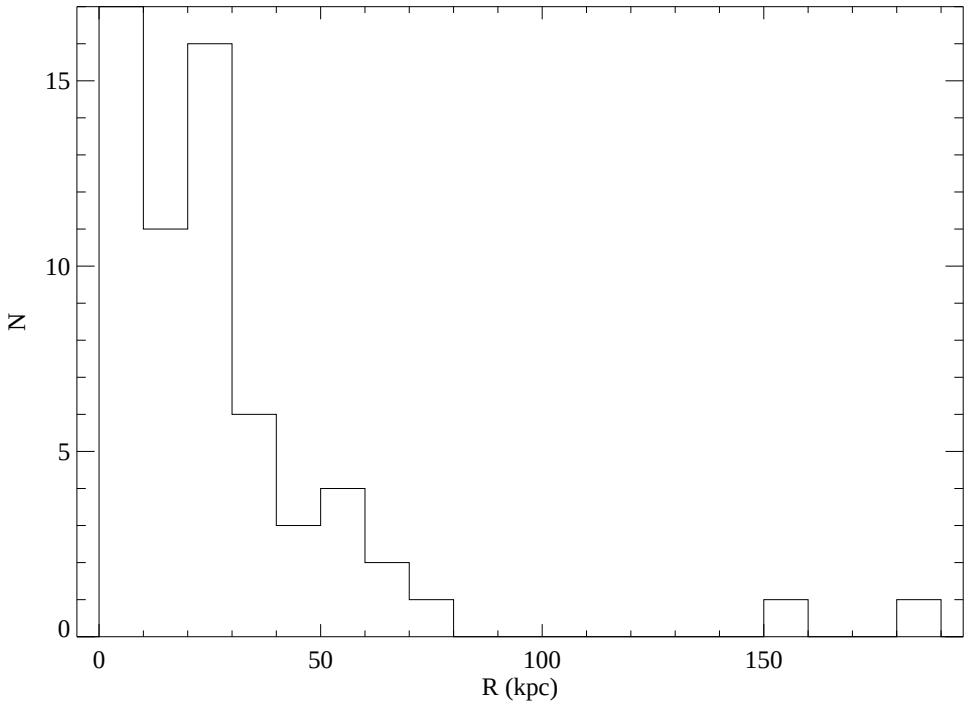

Figure 3: Distribution of cavity distance from the nucleus of the host cD galaxy.

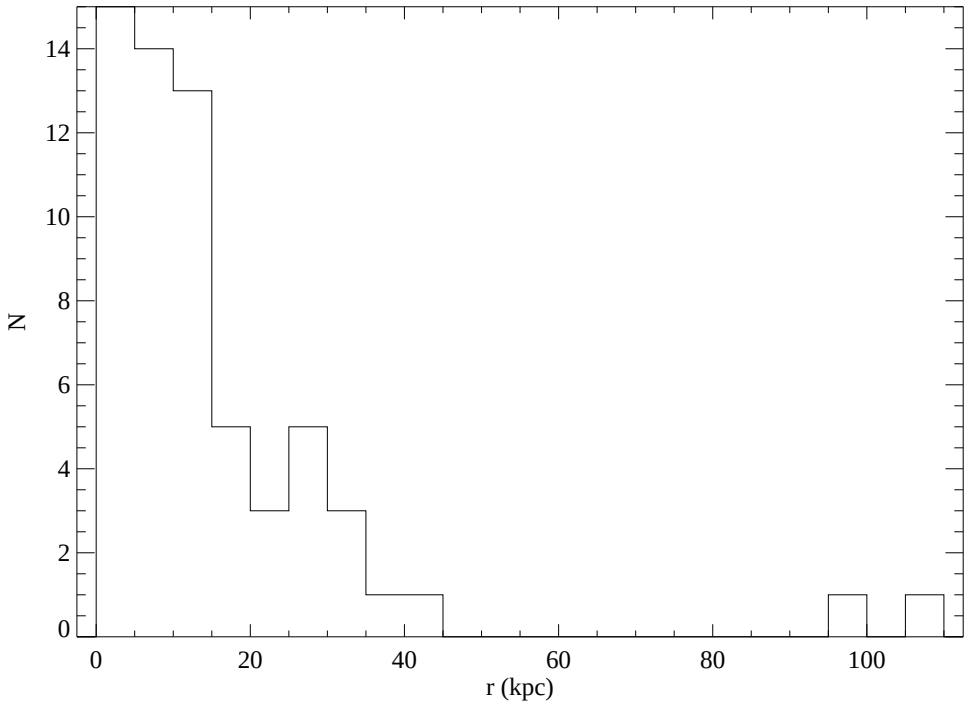

Figure 4: Distribution of cavity sizes. An ellipse was fitted to each cavity and its is size expressed as $\sqrt{ab}$, where a and b are the semiaxes.

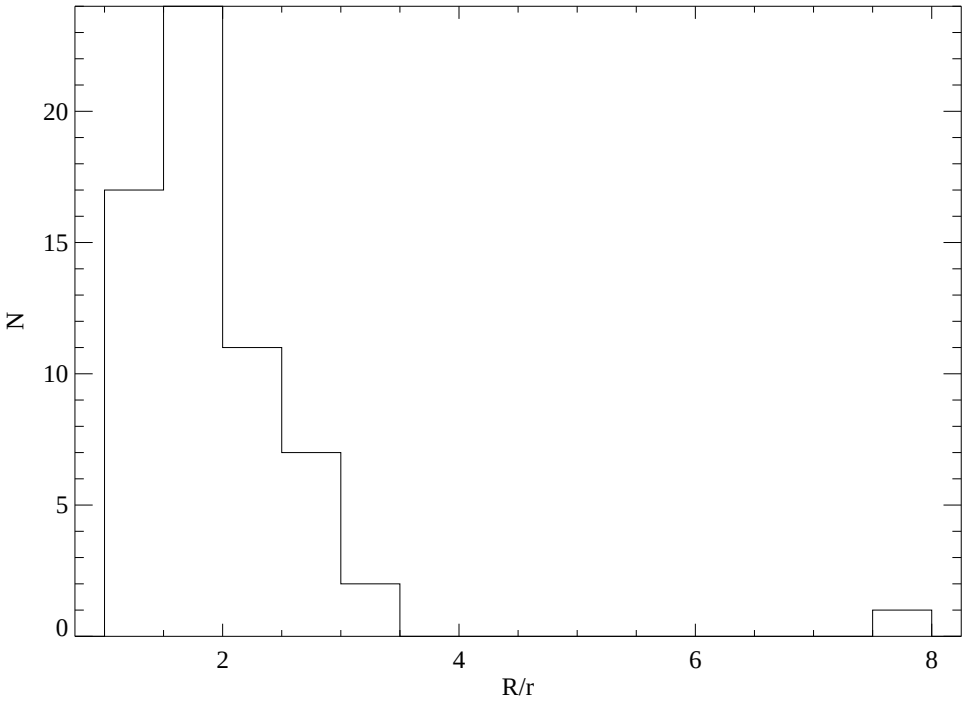

Figure 5: Distribution of the ratio of cavity size to nuclear distance. See Figures 3 and 4.

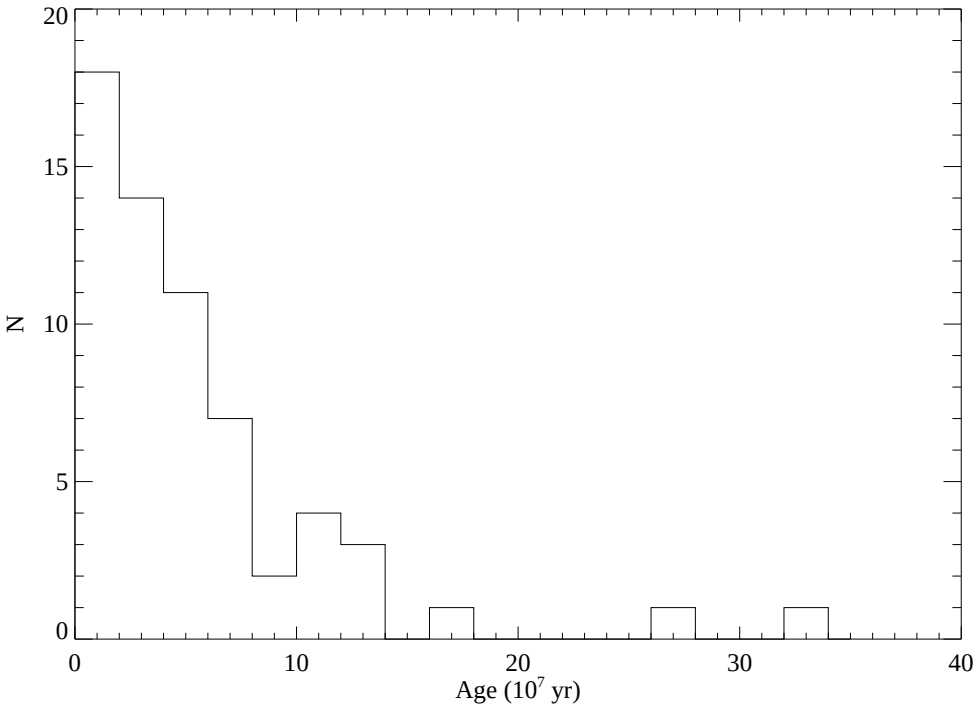

Figure 6: Distribution of cavity buoyancy ages.

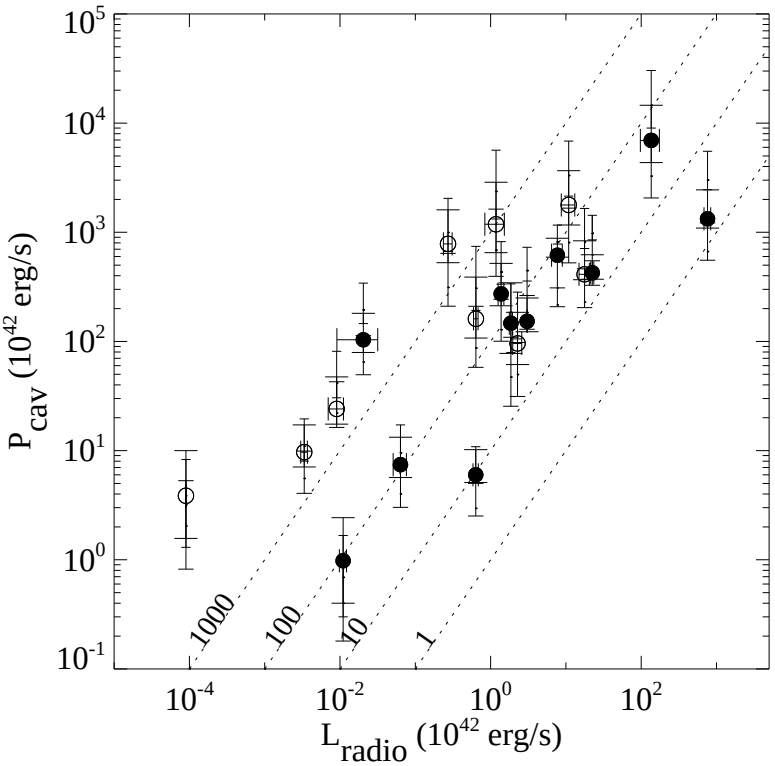

Figure 7: Total radio luminosity (10 MHz – 10 GHz) plotted against jet power ($4pV/t_{\rm bouy}$) taken from Laura Bîzan's PhD thesis (2007). The diagonal lines represent ratios of constant jet power to radio synchrotron power. Jet power correlates with synchrotron power but with a large scatter in their ratio. Radio sources in cooling flows are dominated by mechanical power. The radio measurements were made with the Very Large Array telescope.

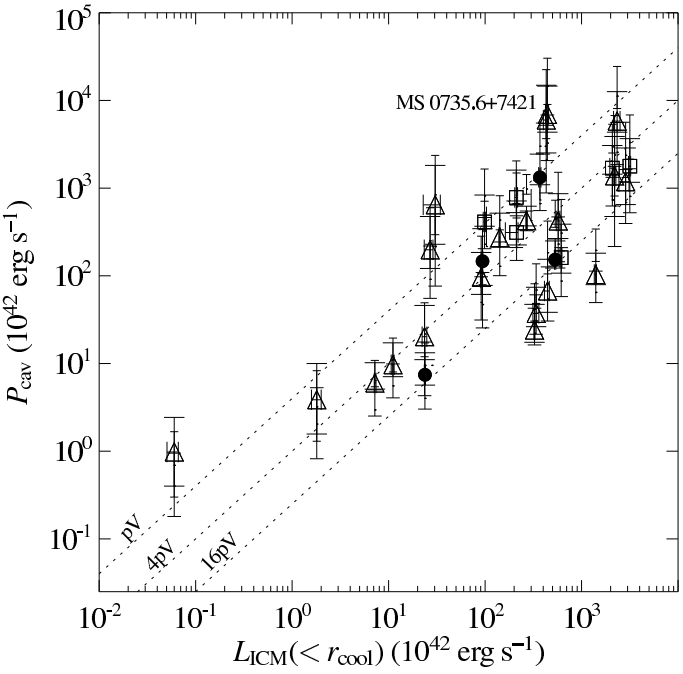

Figure 8: Cavity power of the central AGN plotted against the X-ray luminosity of the intracluster medium (ICM) within the cooling radius, after correcting for mass deposition (Rafferty et al. 2006). The symbols and wide error bars denote values of cavity power calculated using the buoyancy timescale. Short and medium width error bars denote the limits of the cavity power calculated using the sound speed and refill timescales, respectively. Diagonal lines denote equality between heating and cooling rates assuming pV, $4pV$, and $16pV$ of energy per cavity, respectively.

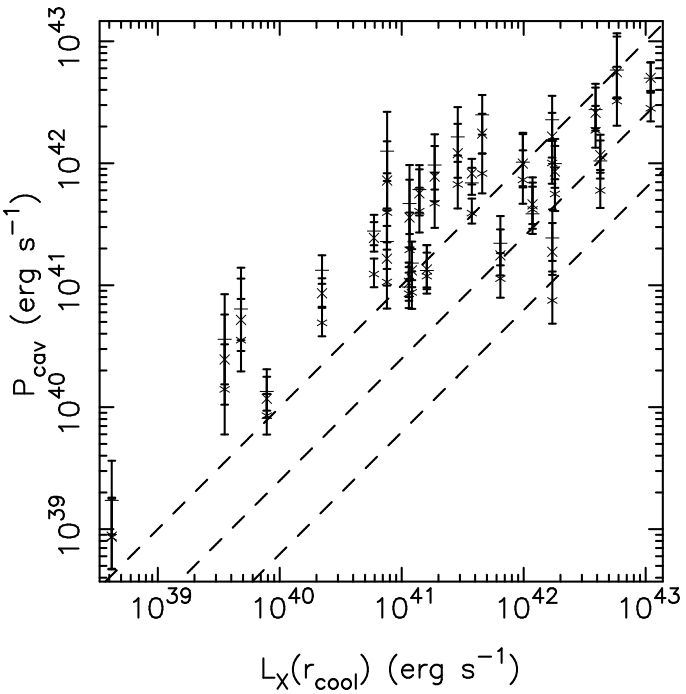

Figure 9: Cavity power versus cooling power for nearby giant elliptical galaxies (Nulsen et al. 2007). Cooling power is the X-ray luminosity from within the projected radius where the cooling time is 7.7×10^9 years. Cavity powers are determined using an energy of pV per cavity and a range of cavity age estimates (see Figure 8). The dashed lines show equality for cavity energies of pV, $4pV$, and $16pV$, top to bottom. All but one system lie above the $4pV$ line, indicating that radiative losses can bebalanced by AGN power.

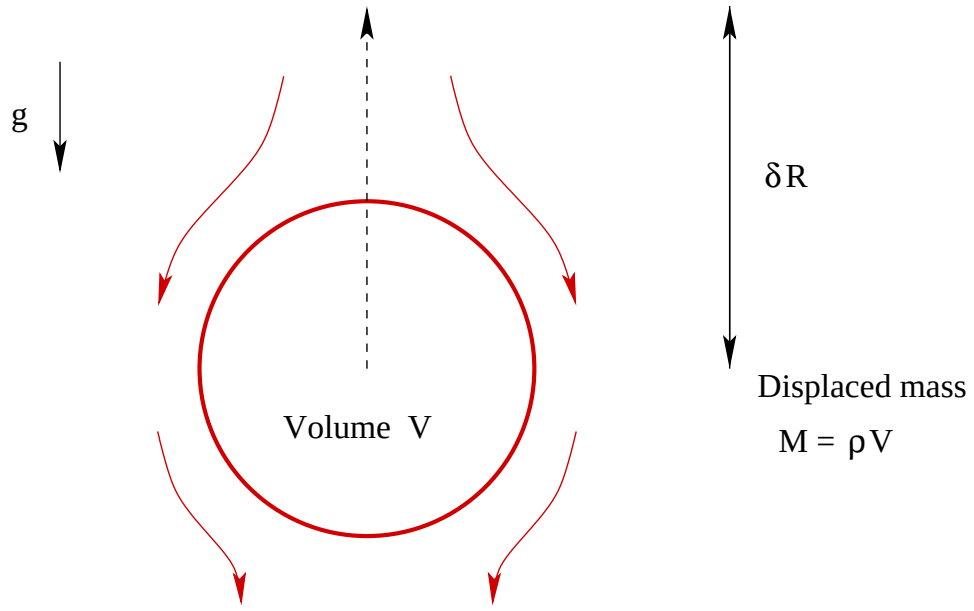

Figure 10: Buoyant cavity. As the cavity rises, gas falls inward to fill the space, turning gravitational potential energy into kinetic energy in the cavity's wake.

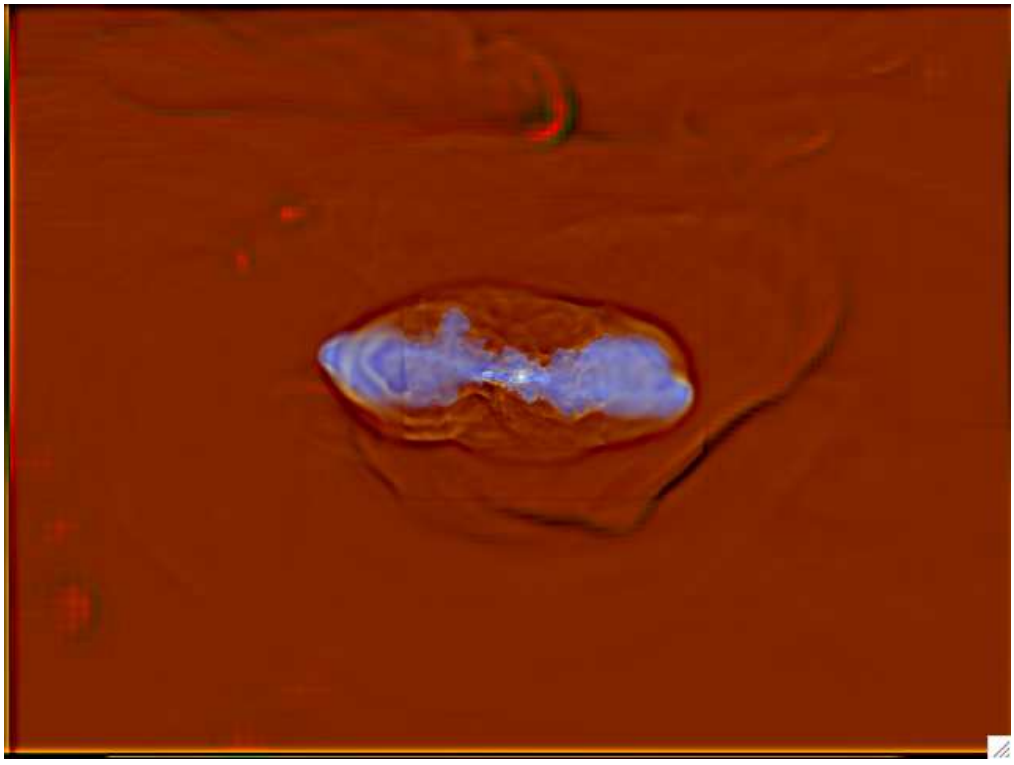

Figure 11: Simulation of jets interacting with the intracluster medium (ICM) from Heinz et al. (2006). Radio synchrotron emission is in blue and X-ray emission in red. This simulation produces a realistic cocoon shock, cavities, and ripples. The strong gas feature to the lower right is an unrelated merger shock. Motion of ICM owing to ongoing cluster growth and wobbling of the Cygnus A-like jet both have a significant impact on the outcome of the model.

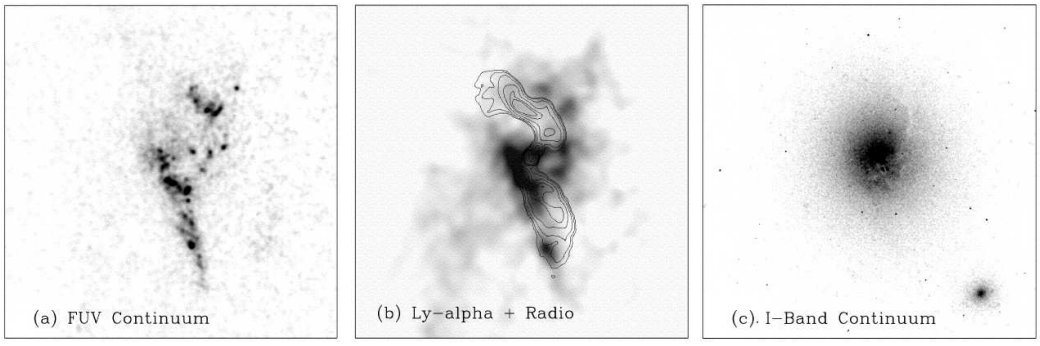

Figure 12: Hubble Space Telescope images of the central 19 × 19 arcsec (24 × 24 kpc) of the cD in Abell 1795 from O'Dea et al. (2004): *Left:* Far-UV continuum, *middle:* Ly emission with radio contours superposed, and *right:* I-band continuum. Note the bright knots of star formation and Ly emission that are seen preferentially along the radio lobes. A dust lane is evident in the I-band image. The star formation rate in this system is 10 – 30 $M_\odot$ year^{-1}.